TECHNISCHE UNIVERSITÄT WIEN
Vienna University of Technology

DIPLOMARBEIT

Effects of Ultrasound induced Cavitation Mechanisms on Biological Systems

durchgeführt am
Institut für Angewandte Physik
der Technischen Universität Wien
Ao.Univ.Prof. Dipl.-Ing. Dr.techn. Martin Gröschl

in Zusammenarbeit mit dem
Department of Radiology
der University of California, San Diego
Associate Prof. Thilo Hoelscher, M.D.

eingereicht von
Maximilian Dirnbacher

Ort, Datum

Unterschrift

Statement of Authorship

I hereby certify that this master thesis has been composed by myself, and describes my own work, unless otherwise acknowledged in the text. All references and verbatim extracts have been quoted, and all sources of information have been specifically acknowledged. It has not been accepted in any previous application for a degree.

Vienna. April 15, 2013

Maximilian Dirnbacher

Acknowledgements

It gives me great pleasure in acknowledging the help of Univ.Prof. Dr. Bernhard Schwaighofer. Research activities abroad at the University of California, San Diego would have been impossible without his help. It is thanks to him that I got to know my external advisor Associate Prof. Thilo Hoelscher, M.D., Director of the *"Brain Ultrasound Research Laboratory"* (BURL) at the University of California, San Diego, two years ago. I owe my deepest gratitude to Associate Prof. Hölscher, M.D. who supported me not only in any work related issue, but also on a very high personal level. His professional competence and the friendship between us were from tremendous advantage for conducting highly effective and valuable research. I would like to thank Ao.Univ.Prof. Dipl.-Ing. Dr. Martin Gröschl who right away agreed to be my internal advisor from the Vienna University of Technology and I very much appreciate his patience in answering general questions relating the thesis and his support concerning any administrative matter. I consider it an honor to work with Arne Voie, Ph.D., who advised me with his enormous technical expertise during the research activities.

This thesis would not happen to be possible without the grant provided by the Austrian Marshall Plan Foundation and I wish to thank all the employees for making my dream to study abroad come true.

I am also indebted to my family and relatives, who supported me mentally and financially (not forgetting the proof-reading)! Furthermore, I would like to thank all my friends who shared fun and bad times with me during my studies and always gave me new motivation for completing this thesis.

Abstract

Modern techniques in neuroscience such as the application of transcranial *focused ultrasound* (FUS) need to be explored in order to diagnose or treat a variety of neurological disorders. Research within this thesis is another big step towards the integration of this technology into regular clinical practice.

Therapeutic applications of FUS cause thermal or non-thermal (mechanical) effects on biological tissue. It is therefore necessary to separate thermal therapy from mechanical therapy, whereas the first form is related to the physical property "intensity", the latter to "pressure".

All measurements presented in this work were performed using two human cadaver skulls. One of the main aims of this thesis was to determine two different volumes per skull. These two volumes were termed the *"thermal-therapy" treatment envelope* (TE) and the *"mechanical-therapy"* TE based on their underlying effect. According to Baron, Aubry et al. (2009) intensity is proportional to the square of the *peak negative pressure*, which led to the assumption that the *"mechanical-therapy"* TE describes a larger volume within the skull than the *"thermal-therapy"* TE. This theory has been proved by the measurements of the acoustic field distribution within the skulls.

Furthermore, additional measurements on the *"mechanical-therapy"* TE, especially on the important mechanical effect of *cavitation* without or in combination with *microbubbles* (MB) were performed. These *cavitation* studies included the development of a *passive cavitation detection* (PCD) method by that the threshold in *peak negative pressure* for a *cavitation* event was determined. Results not only proved the correctness of the *treatment envelopes* they also demonstrated that the threshold for a *cavitation* event was significantly lower if *MBs* were present.

All in all, this research suggests that a mechanical based therapy (e.g. *cavitation*, particularly with MBs) might be applied to brain regions beyond the capability of thermal based applications (e.g. tumor ablation). This knowledge could be of high practical relevance for any new FUS technology in the field of neuroscience.

Kurzfassung

Es ist von größter Bedeutung, die Forschung an modernen Techniken im Bereich der Neurowissenschaften voranzutreiben. Ein Beispiel dafür ist die Entwicklung einer transkraniellen Anwendung von fokussiertem Ultraschall, die es ermöglicht neurologische Erkrankungen zu behandeln. Die zugrunde liegende Forschungstätigkeit für diese Diplomarbeit trägt maßgeblich dazu bei, eine solche Technik im klinischen Bereich zu etablieren.

Therapeutischer Ultraschall kann entweder einen "thermischen" oder "nicht-thermischen" (mechanischen) Effekt auf biologisches Gewebe bewirken. Es macht durchaus Sinn, aufgrund dieser zwei Effekte, eine thermische Therapie von einer mechanischen Therapie zu unterscheiden, wobei die erste Form mit der physikalischen Größe „Intensität" und die zweite mit der physikalischen Größe „Druck" verbunden wird.

Alle Messungen wurden an menschlichen Schädelknochen von Leichen durchgeführt. Eines der Hauptziele dieser Forschung war es, zwei akustische Volumina innerhalb eines Schädelknochens zu definieren. Diese Bereiche, die sogenannten *Treatment Envelopes* (TE), wurden anhand ihres zugrunde liegenden Effekts in einen *"thermisch-therapeutischen"* TE und einen *"mechanisch-therapeutischen"* TE unterteilt. Die Tatsache, dass laut Baron, Aubry et al. (2009) Intensität proportional dem Quadrat des negativen Spitzendrucks ist, führte zur Annahme, dass der *"mechanisch-therapeutische"* TE ein größeres Volumen im Schädel als der *"thermische-therapeutische"* TE beschreibt. Diese Theorie konnte in der Praxis bewiesen werden.

Des Weiteren wurden Messungen am *"mechanisch-therapeutischen"* TE durchgeführt. Im Speziellen wurde dabei der äußerst wichtige mechanische Effekt der *Kavitation* in An-/ und Abwesenheit von *Mikrobläschen* erforscht. Die eigens dafür entwickelte Methode der *passiven Kavitations Detektion* ermöglichte es, Grenzwerte für *Kavitation* zu definieren. Nicht nur die Richtigkeit der TEs konnte damit bewiesen werden, es war auch möglich, den Einfluss von *Mikrobläschen* auf den Grenzwert zu demonstrieren. Dieser ist, wie vermutet, niedriger, wenn *Mikrobläschen* anwesend sind.

Die durchgeführte Forschungsarbeit führt zur Annahme, dass eine Therapie basierend auf den mechanischen Effekten (e.g. *Kavitation*, v.A. in Anwendung mit *Mikrobläschen*) einen größeren Wirkungsbereich in der Hirnregion als eine thermisch-basierte Anwendung (e.g. Tumorablation) haben sollte. Diese Erkenntnis ist von großer Bedeutung für jegliche Entwicklung von Anwendungen des fokussierten Ultraschalls im Bereich der Neurowissenschaften.

Table of Contents

1 Introduction

The application of *focused ultrasound* (FUS) as a therapeutic approach has become a promising method to create clinical effects within the body non-invasively. Since stroke is one of the most frequent acute diseases with fatal outcome worldwide (2nd common cause of death), research in the field of neuroscience to improve stroke care is particularly important. The accepted gold standard of acute stroke treatment is the intravenous administration of *tissue Plasminogen Activator* (tPA). Due to its risk profile and its potential side effects less than 3% of the stroke population receive tPA, underscoring the significant limitations of this approved therapy. Hence, there is a high demand for innovative treatment options in stroke care in combination with or in absence of tPA. First results using non-invasive transcranial FUS for stroke therapy have shown great promise in this regard. The research done for this thesis contributes to such a technology, providing significant, new knowledge how FUS could be used efficiently and safely for neurological brain diseases, such as stroke.

Apart from stroke therapy recent research focuses on the opening on the *blood-brain barrier* (BBB) non-invasively using transcranical FUS. Delivery of therapeutic and diagnostic agents to the *central nervous system* (CNS) is limited by the BBB. The function of this specific structure in the brain, which is formed by vascular endothelial cells, is to act as a barrier to the diffusion of substances, i.e. enzymes, genes, or drugs from the vascular space to the CNS tissue. The probability of an agent to pass the BBB varies with its size and lipid solubility. Without any additional help lipid soluble small-molecule agents are more likely to pass this barrier by free diffusion. These active substances might be used to treat diseases such as depression or chronic pain. Contrary to this, most of the CNS disorders, particularly neurodegenerative diseases e.g. Alzheimer disease and Huntington disease demand for large-molecule agents that will not cross the BBB without optional mechanisms of delivery.

Still, FUS entails considerable risks to the human body that need to be eliminated. Research done for this thesis is necessary in order to detect, characterize and most important to control various effects caused by the application of FUS on the human brain. Overall goal is to achieve therapeutic intensities in the focal volume on the one side but on the other side to keep the intensity to a minimum in the unaffected tissue. To accomplish this goal the knowledge of basic mechanisms as well as the acoustic

properties inside the skull, being exposed to a FUS sound field, are required. Since *cavitation* mechanisms have been described to induce therapeutic effects in combination with FUS, the knowledge about the interplay between *cavitation* events and transcranial sound field characteristics is of utmost importance (Bailey, Khokhlova et al. 2003). Formerly feared as a significant risk factor, there is growing evidence that *cavitation* mechanisms are considered to induce mechanical (therapeutical) effects. *Cavitation* detection requires the assessments of acoustic pressure in the target area, which was part of the present project. Moreover, the simple relationship between acoustic pressure and intensity makes the acquired data useful for research on thermal effects. To date, thermal ablation is the leading mechanism for the medical use of FUS in non-invasive disease treatment. Besides extensive acoustic sound field characterization using transcranial FUS potential attenuation, scattering, and absorption effects, caused by transskull FUS insonation were studied.

The performed research in this thesis demonstrates that *cavitation* is related to pressure, whereas the thermal effect depends on intensity. It is shown that the thermal effect has an underlying acoustic cause and that specific acoustic parameters can be identified. Furthermore, results suggest that applications using the *cavitation* mechanism for a therapeutic purpose may be able to treat regions in the tissue that cannot be reached by thermal-based applications.

1.1 Therapeutic Ultrasound

Diagnostic ultrasound is a widely used and a well-known imaging modality in today's medicine. The idea of applying ultrasound as a treatment method (therapy) is not new at all and currently a lot of research is done to invent or improve techniques due to many beneficial properties of ultrasound. One of the advantages of ultrasound waves is the possibility to focus them tightly (FUS) and by doing that to deliver the sound energy to a certain point in the biological tissue without any effects on the tissue outside the focus (Figure 1).

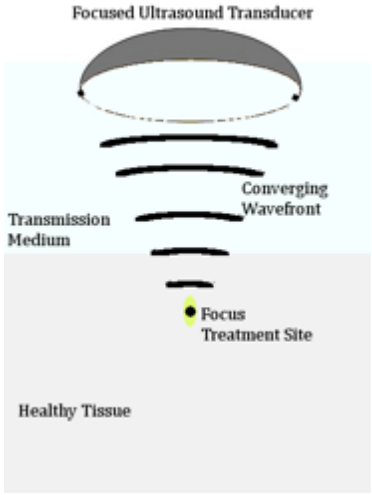

Figure 1: FUS principle.

The application of FUS allows performing a variety of highly precise operations due to a sharp achievable focus. Still, in current medicare applications FUS is not utilized to its full potential yet and research strives to develop innovative techniques and new applications.

1.2 Applications of Focused Ultrasound in Neuroscience

The capability of FUS to achieve a spatial resolution at millimeter precision keeping the effects on the surrounding tissue to a minimum at the same time makes its application in neuroscience attractive. This is why recent research on new procedures to treat neurological conditions like *thrombolysis* within the brain (i.e. stroke therapy) (Behrens, Spengos et al. 2001, Burgess, Huang et al. 2012), the reversible disruption of the BBB (Hynynen, McDannold et al. 2005, Vykhodtseva 2010, McDannold, Arvanitis et al. 2012) or the ablation of brain tumors (Tobias, Hynynen et al. 1987, Hynynen and Jolesz 1998, Tanter, Thomas et al. 1998, Aubry, Tanter et al. 2003, Aubry, Marsac et al. 2010), is getting more and more prominent.

Of course the application of FUS is not limited to transskull therapy, but due to the fact that research within this thesis concentrates on FUS on the human skull, other applications beside the ones mentioned above, will not be discussed.

1.2.1 Stroke Therapy

Stroke is an acute, sometimes even life threatening event. Therefore, this situation requires fast and accurate diagnostic tools and therapy efforts – "Time is Brain". The vascular system of the brain (Figure 2) consists of 2 major arterial inputs on the left and

right side of the brain – the common carotid artery and the vertebral artery. The common carotid artery gives rise to the internal carotid artery and continues to its intracranial bifurcation into the medial (middle) and anterior cerebral artery. The anterior cerebral artery provides blood supply to parts of the frontal and parietal lobe, as well as the rostral part of the temporal lobe, the diencephalon, and the eyes. The medial cerebral artery provides blood supply to the frontal and parietal lobe. The vertebral artery gives rise to basilar artery that bifurcates into the posterior cerebral artery. The latter provides blood supply to the occipital and temporal lobe (www.strokecenter.org).

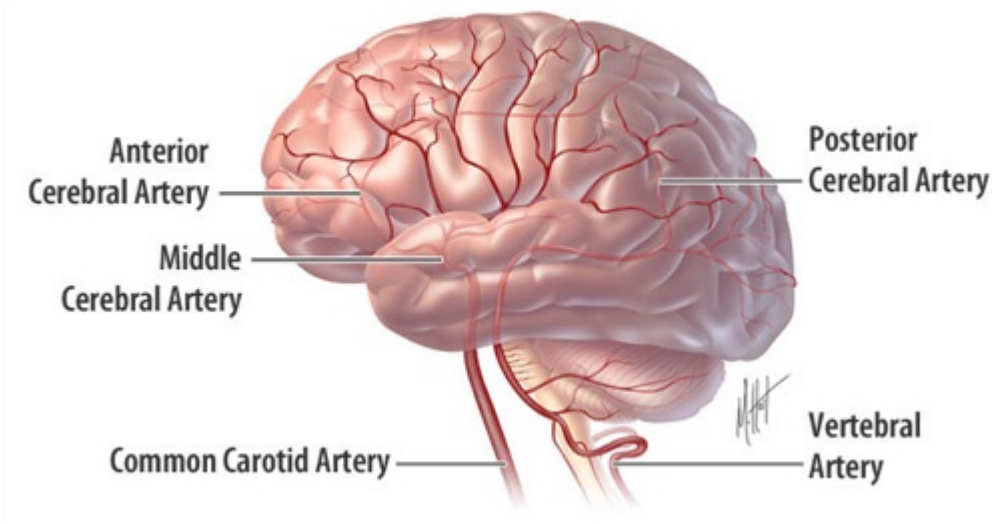

Figure 2: Vascular system of the brain (www.strokecenter.org).

One distinguishes between different forms of stroke. The ischemic stroke (Figure 3) is caused by a thrombus or thrombo-embolic event – i.e. a smaller branch of one of the major arteries is clogged by a thrombus, thus blood circulation in a circumscribed region stops. A thrombus clogging a branch of one of the major arteries may be up to several millimeters in size.

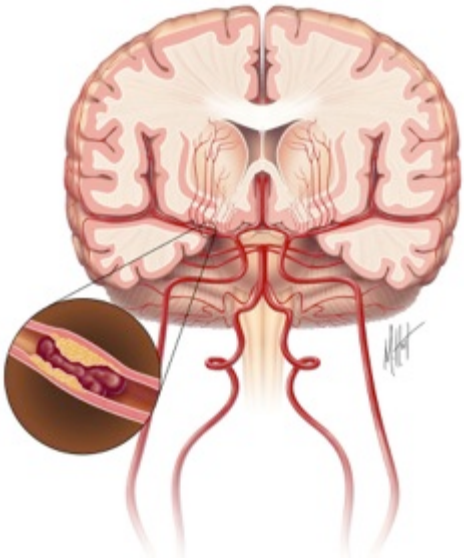

Figure 3: Ischemic stroke due to blocked artery in the brain (www.strokecenter.org).

Due to the anatomical branching of the vascular system the majority of ischemic strokes occur within the middle cerebral artery and its branches. Less often ischemic strokes occur in the region of the anterior or posterior cerebral artery. Under some conditions an ischemic stroke might convert into a hemorrhagic stroke (Figure 4) – e.g., after an initial ischemia a bleeding into brain tissue occurs due to high blood pressure and pathological changes of blood vessel as it is the case for example in amyloidosis.

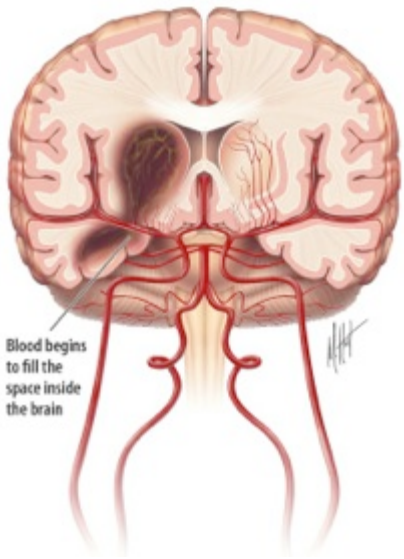

Figure 4: Intracerebral Hemorrhage (www.strokecenter.org).

Contrary to an ischemic stroke rupture of a blood vessel leads to a hemorrhagic stroke, which is an intracerebral bleeding that interrupts blood circulation. Additionally the blood outside the vessel may destruct brain tissue (Zeiler and Auff 2007). Figure 5 shows an example of a cerebral infarction on the left side (hemisphere) of the brain visualized by two different diagnostic imaging modalities.

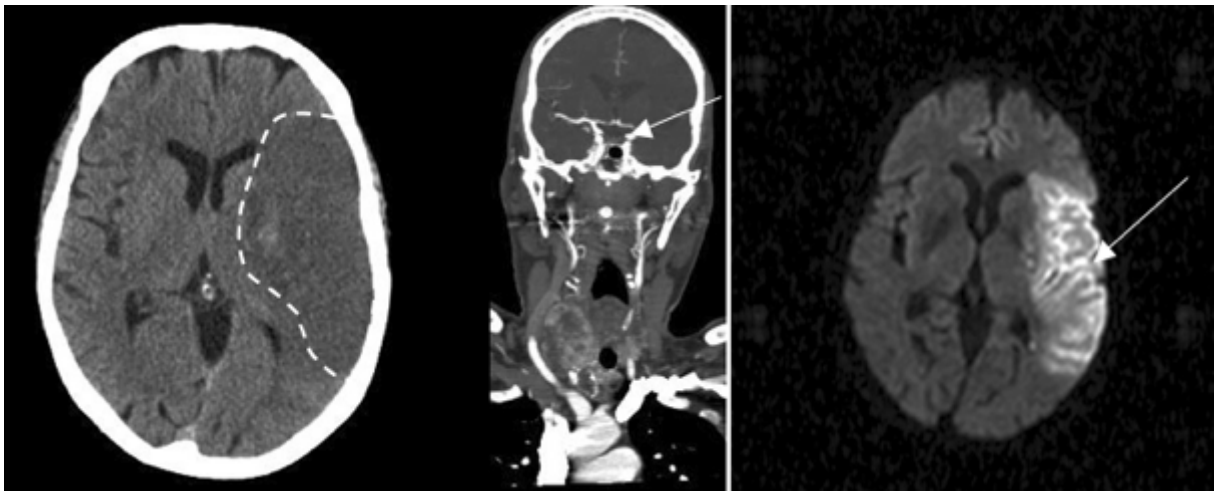

Figure 5: Example of a cerebral infarction on the left hemisphere due to a M1 thrombosis of the middle cerebral artery: computed tomography (CT) scan with a demarcation zone (left side), CT-angiography which shows a stop of flow (see arrow in the middle), DW-MRI (diffusion weighted-magnetic resonance imaging) which shows the extend of edema caused in the zone of tissue infarction (courtesy Department of Neuroradiology, Medical University of Vienna).

In current stroke therapy a strict protocol should be followed, since successful acute treatment – i.e. thrombolysis (the breakdown of blood clots) has to be established within a time window of 4.5 hours from the onset of first neurological symptoms. The immediate steps are a neurological examination and evaluation according to the *National Institute of Health stroke scale* (NIHSS), blood test and a computed *tomography* (CT) scan with angiography or if possible a *magnetic resonance imaging* (MRI) scan, to distinguish the type of stroke and locate it. In case of an ischemic stroke thrombolysis with intravenous *recombinant plasminogen activator* (r-tPA) can be used to dissolve the thrombus. In certain cases intra-arterial thrombolysis is an alternative or additional method for dissolving a thrombus. In this case the r-tPA is administered via a small catheter introduced into the arterial system at the immediate vicinity of the thrombus. Even if this procedure is not successful, a thrombus might be extracted by a so called retriever catheter (Broderick, Palesch et al. 2013, Ciccone, Valvassori et al. 2013).

All of these procedures need the efforts of specialized hospitals and medical personnel. Furthermore, the use of r-tPA for thrombolysis might be hazardous since

bleeding can occur in any part of the circulatory system. It is understandable that the use of r-tPA has strict restrictions, and therefore cannot be used in every stroke patient (Veltkamp 2012).

In the case of ischemic strokes transcranial FUS in combination with *microbubbles* (MB) may represent a potential method to restore the normal flow by complete fragmentation of the blood clot without r-tPA or at least accelerate clot lysis in conjunction with r-tPA (Behrens, Spengos et al. 2001).

1.2.2 Drug Delivery (Opening of Blood-Brain Barrier)

Delivery of therapeutic and diagnostic agents to the CNS, i.e. the brain and spinal cord, is limited by the BBB (Figure 6). The function of this specific structure in the brain, which is formed by a combination of vascular endothelial cells, pericytes and astrocytes is to act as a barrier to the diffusion of substances, i.e. enzymes, genes, or drugs from the circulating peripheral blood to the CNS. It therefore regulates and optimizes the cerebral function. The probability of an agent to pass the BBB varies with its size and lipid solubility. Without any additional help lipid soluble small-molecule agents are more likely to pass this barrier by free diffusion. These active substances might be used to treat diseases such as depression or chronic pain. Contrary to this most of the CNS disorders, particularly neurodegenerative diseases, e.g. Alzheimer's disease and Huntington's disease demand for large-molecule agents that will not cross the BBB unaided. As a result they remain intractable (Hawkins and Davis 2005).

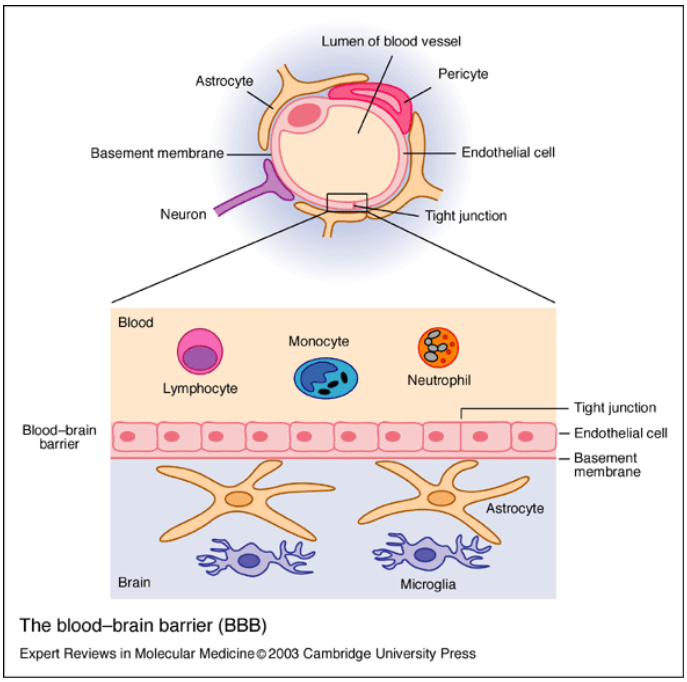

Figure 6: Schematic figure of the blood-brain barrier (BBB). The close up of the blood vessels wall shows that endothelial cells are tightly linked together and create a barrier (i.e. the BBB) between the circulation and the brain parenchyma (e.g. astrocytes or microglia) (Francis, van Beek et al. 2003).

This fact emphasizes the necessity of a technique to open the BBB. A broad literature proofs that a high potential to open the BBB transcranially, locally and non-invasively is attributed to FUS and, more so, FUS in combination with MBs. Nevertheless, questions regarding application safety and efficacy remain to be answered.

1.2.3 Brain Tumor Ablation

A general literature review showed that currently various methods are involved in brain tumor ablation. Drawbacks of these applications are, for example the exposure of the patient to ionizing radiation, administration of chemotherapeutic agents or the invasive treatment of the brain lesion, which entails considerable high risks.

Due to the beneficial properties of FUS (see 1.1), localized tissue ablation within the brain in order to destruct a tumor might be possible. Still, as it will be discussed in 2.2.2, thermal (skull heating) and mechanical (*cavitation*) components mainly contribute to the today's low acceptance of FUS as a medical treatment option.

Using a combination of transcranial FUS and MRI to perform a non-invasive treatment surgery, so called, transcranial MRI-guided FUS surgery (TcMRgFUS), addresses at least the thermal concern. In this case the transcranial FUS treatment is planned and guided

by MRI. This allows, for example, to localize the tumor and monitor the temperature distribution within the tissue in real-time (McDannold, Clement et al. 2010).

1.3 Cavitation

Disregarding potential FUS applications, research on *cavitation* was mainly of interest in areas different from medicine. Any propeller, turbine or pump is capable to cause *cavitation* as this phenomenon, in general, occurs once, a liquid is subjected to low pressure, i.e. the depressurization of the liquid. *Cavitation* detection was of particular importance during wartime when ships or submarines should remain untraceable by enemies. As a matter of fact *cavitation* by a propeller may increase the noise level for about 20-40dB, which could be detected by underwater listening devices (i.e. hydrophone). Another concern is the effect on a rotational device (e.g. turbine) as *cavitation* causes major wear and even damage. As a result, the affected part loses its level of performance (Lecoffre 1997). Research in this field shows great effort in product design in order to prevent *cavitation*.

As discussed above, *cavitation* phenomena might cause harmful effects during occurrence in living organisms. Specifically for medical applications using FUS is of crucial importance to recognize cavitation mechanisms and preferably to have the ability to predict and control these.

2 Theory

2.1 Biological Effects on Tissue by Application of Focused Ultrasound

Effects on tissue caused by FUS can be classified as either thermal or non-thermal effects. In general both effects are due to vibration or rotation of the molecules within the insonicated volume. The resulting effect depends on the size of the participating molecules and the medium. As a matter of fact the thermal effect occurs if the system is fluid and the molecules are relatively small (Hill, Bamber et al. 2005). In the case of therapeutic FUS the desired effect is to cause a temperature rise (thermal effect) in the focal volume, whereas the tissue near the transducer remains unaffected. By focusing ultrasound it is possible to position the focal volume and as a result to evoke this thermal effect at a specific site within the body. In general a temperature elevation to approximately 40°C at a specific point in the human body is called hyperthermia. Possible effects caused by hyperthermia are

> *increased cell membrane permeability and a lowering of the pH level within the cytoplasm, as well as bulk effects such as ischemia and lack of perfusion* (Hendee 2012).

The capability of FUS to generate a temperature rise up to 70°C at the focus within a short time demonstrates the potential of the application. Such rapid changes in temperature might be a way to ablate tissue (e.g. tumors) by causing coagulative necrosis (cell death). A drawback of this procedure is the difficulty to monitor and control the temperature rise (Tu, Ha Hwang et al. 2012).

Still, according to Hendee (2012), FUS represents a technique to ablate tumors by rapid temperature elevation. In this case the thermal effect is thought to cause proteins to denature (i.e. when the protein looses its secondary and tertiary structure).

Johns (2002) compares the two different therapeutic effects of ultrasound and shows that the non-thermal effect usually is a combination of *cavitation* and acoustic streaming. The latter is described as a steady flow of ions and small molecules that is caused by an ultrasonic wave propagating through a fluid (acoustic streaming will be discussed more detailed in 2.2.2). However, acoustic streaming is the driving force that moves free-floating molecules unidirectional around stationary cell structures.

Cavitation on the other side may affect the activity of the cell or change the cell function. Non-thermal effects on biological tissues are more a combination of *cavitation* and acoustic streaming due to the fact that a clear distinction whether *cavitation* or acoustic streaming caused the biological effect is difficult. In vitro studies showed that effects are growth retardation of cells, increase in protein synthesis, and membrane alterations. This means that ultrasound basically harms the cell first in a way that the cell slows down in growing. As usual the cell starts a cellular recovery response and therefore increases its protein synthesis (production).

2.2 Focused Ultrasound

2.2.1 The Function Principle

2.2.1.a Transducer

In FUS the beam pattern and the shape of the focal point mainly depend on the transducer design. Some properties of a transducer that contribute to this are pointed out here. Note that a transducer delivers sound energy in form of pressure waves (whereas in the case of X-Ray for example electromagnetic energy is transmitted by the movement of photons).

The aim of FUS, particularly in neuroscience, is to deliver sufficient high acoustic energy to a small target zone (i.e. focal point). To achieve this goal factors such as the operating frequency, the transducers aperture and focal depth, convenient acoustic coupling methods, the waveform selection or amplifier characteristics should be considered carefully during design of a transducer (Keilman and Kaczkowski 1998). The influence of the operating frequency on several acoustic parameters will be discussed in detail in section 2.2.1.b.

Maintaining a sharp focal zone and controlling the focal distortion becomes especially challenging if the acoustic beam hits bone. The effect of bone on attenuation and scattering of ultrasound, on the focus and as a result on the delivered energy will be shown in the following chapters.

The properties frequency and diameter of the transducer are known to determine the length of the near field and the divergence of the far field. Increasing transducer diameter and frequency results in an increasing length of the near field, whereas the divergence of the far field decreases (Hendee and Ritenour 2002). Note that

the transition between the near and far field is sometimes referred to as the “natural focus”. Within the thesis the term will be used frequently.

2.2.1.b Frequency

One of the key parameters of FUS is the operating frequency, which is usually in the higher Kilohertz (kHz), or lower Megahertz (MHz) range. Several properties change with frequency, e.g. the depth of penetration decreases as the frequency increases. Furthermore, Yin and Hynynen (2005) showed that by increasing the frequency ultrasound is absorbed more which results in a higher energy conversion from acoustic to thermal energy.

The tissue-specific attenuation coefficient α defines the attenuation of ultrasound energy. This coefficient mainly depends on the absorption of the energy, i.e. basically the conversion of acoustic energy to other forms of energy, and on scattering of the energy (scattering of the energy in many directions other than its original direction of propagation). These two mechanisms contribute to the attenuation coefficient. For bone the attenuation coefficient is very high in comparison to soft tissue. According to the definition, from the higher coefficient it is evident that there is more attenuation in bone than in soft tissue. The units of the attenuation coefficient are Nepers (Np) per unit length, whereas one Neper equals -8.69 decibels (dB) of gain. α is therefore either given as Np/length or dB/length (Howard and Graham 2003).

It is of utmost importance to mention that the attenuation coefficient α has a frequency dependence in the way that α increases almost linearly with frequency (Hendee and Ritenour 2002). Furthermore, the attenuation rate indicates the relationship between penetration depth of ultrasound and the operating frequency. For higher frequencies ultrasound loses power in propagation direction more rapidly than for lower frequencies (Quistgaard, Desilets et al. 2010).

The effect of the frequency on the focus has been observed in different studies, e.g. by Rosenschein, Furman et al. (2000). As shown, the shape of the focus point changes with frequency due to the fact that frequency and wavelength are inversely proportional. It has been proven that the focal area decreases in size at higher frequencies. Common frequencies used for FUS are 1 MHz, 650 kHz or 220 kHz.

2.2.2 Thermal Effect and Mechanical Effect

Bioeffects of ultrasound are separated into thermal and mechanical effects:

Thermal Effect:

Energy absorption in general results in the conversion of acoustic waves into thermal energy. The ultrasound starts to heat up the medium- i.e. the thermal effect. Ultrasound can change the properties of tissue by inducing a temperature rise. The extent of such a thermal effect depends on different tissue properties, e.g. the type of tissue (muscle, bone, etc.), the blood perfusion, the density, the absorption, reflection, and attenuation coefficient, furthermore on the ultrasound field configuration, e.g. the spatial and average intensity, the power, the transmission duration, the mode (pulsed or continuous waved) as well as the frequency. Some of these factors are linked together and influence the amount of heat production within the body. Especially at the skin-skull bone interface the combination of high attenuation in the bone and the large reflection coefficient of it makes it difficult to predict or control the resulting thermal effect. According to Hynynen and Jolesz (1998), in case of short pulses, absorption of the ultrasound power and the size and shape of the focal spot contribute mainly to the thermal effect and enhance possible thermal damage. To calculate the rate of temperature rise dT/dt at the beginning of an ultrasound pulse, Hynynen and Jolesz (1998) use an equation derived by Nyborg (1981)

$$\frac{dT}{dt} = \frac{< q_v >}{\rho c} \qquad (1)$$

where $< q_v >= \frac{\alpha P^2}{\rho v}$. $< q_v >$ is the temporal average of q_v, which is the instantaneous rate per unit volume at which heat is produced in a medium by an ultrasonic field. As a conclusion the temperature rise can be evaluated from the pressure amplitude of the acoustic field P and is influenced by

> *the density ρ (ρ_{Skull} ~1380-1810kg/m3; ρ_{Brain} ~1030kg/m3)(Wells 1997), the amplitude absorption coefficient α (α_{Brain}=5 Np/m/MHz; α_{Skull} =50 Np/m at 0.5 MHz; and α_{Skull} =300 Np/m at 1.5 MHz if all attenuated energy is assumed to be*

absorbed) (Goss et al. 1978, 1980), the speed of sound ν and the specific heat c of the medium (c_{Brain}=3.9 kJ/kg/°C; c_{Skull}=2.1–2.7 kJ/kg/°C) (NCRP 1992)
(Hynynen and Jolesz 1998).

Noteworthy is the fact that ultrasound may produce heat only at the focal point - that means it can cause a very localized temperature rise. Due to the high-energy deposition and the rapidly increasing temperature at this locality, the duration of sonication must be short (i.e. short exposure time) to protect the tissue against undesirable blood flow or perfusion effects (Deane and Lees 2000, Abramowicz, Barnett et al. 2008). In fact tissue with a high perfusion rate damps the heat generation as heat is distributed away from the focal point. This is of particular importance within the brain, where the metabolism is very high (Billard, Hynynen et al. 1989) and the tissue is delicate and vulnerable.
Studies by Gallo, Draper et al. (2004) demonstrated that the thermal effect depends on the emission modality (pulsed-wave (PW) or continuous wave (CW) ultrasound) as well, whereas CW ultrasound is more likely to heat up tissue.

Recent research by the Focused Ultrasound Foundation (www.fusfoundation.org) showed that the penetration depth of ultrasound decreases with increasing frequency. Due to the higher absorption of high-frequency ultrasound by the skull bone, the thermal energy deposition near the calvarium (top of the skull) will increase. As a consequence, one approach to treat for example lesions closer to the calvarium, would be to select a lower frequency (~230 kHz) in order to keep the conversion of acoustic to thermal energy to a minimum on the skull surface. Lower frequency also leads as previously mentioned to a larger focal zone and a lower attenuation of the ultrasound wave. This results in a lower temperature rise at the focal point and suggests the application of higher ultrasound power if a heat generation at the focal zone is desired. Yin and Hynynen (2005) address the problem that this higher energy passing through the skull bone results in skull heating. This all implicates that different applications require different operating frequencies in order to transmit ultrasound to the desired depth in the tissue and control the heating of the skull at the same time.

In literature thermal effects are divided into two types: tissue can either be heated up by ultrasound over a longer period of time (hyperthermia) or can be ablated by a highly localized high temperature rise (thermal ablation). Figure 7 shows the dependence of temperature elevation from the exposure time.

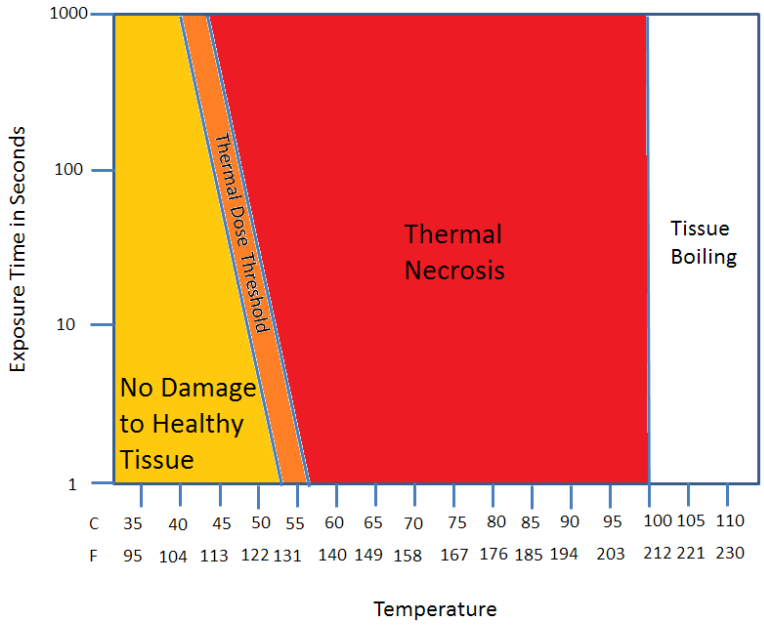

Figure 7: Temperature rise in Celsius (°C) and Fahrenheit (°F) due to exposure time in seconds and the resulting thermal effect on tissue (www.fusfoundation.org).

Common hyperthermia caused by radio-frequency, microwaves, or even ultrasound has major disadvantages compared to FUS: it is very time consuming (duration~1h) and the temperature distribution has to be kept almost constant in a small area, which is not trivial to achieve. In addition, due to the blood flow, temperature within the vessels varies and cold spots may occur. On the contrary FUS produces a high temperature rise at the small focal point for a couple of seconds. Because of this high energy deposition within a short period the treatment time is minimized and blood flow does not have an influence on the temperature distribution. Microscopy of the treated volume shows that the boundary between intact cells and those that were undergoing necrosis by FUS is very sharp (Ter Haar 2001). This proves again the main advantage of FUS, which is the well-defined region of necrosed tissue. The destruction of the tissue by the thermal effect is the usual biological response of tissue if it undergoes rapid heating, i.e. the denaturation of the cells proteins that in extension leads to thermal coagulation and necrosis. According to Barnett, Rott et al. (1997) the absorption coefficient is related to

the protein content of the tissue in the way that a low protein content tissue (e.g. in blood and fat) absorbs less ultrasound energy than one of a larger protein content.

Mechanical Effect:

As previously mentioned, FUS may also have mechanical, non-thermal, effects on tissue based on the fact that ultrasound in general propagates through tissue as a mechanical pressure wave that increases and decreases in amplitude. These changes in pressure may lead to mechanical effects. This kind of effects can be divided into *cavitation*al and non-cavitational effects. *Cavitation* receives the most attention due to its importance for this thesis and will be discussed in 2.3. In this part non-cavitational effects and their underlying mechanisms of action such as radiation force, radiation torque or acoustic streaming will be discussed.

To get a broad understanding of radiation force and acoustic streaming, the property *radiation pressure* has to be explained. If an acoustic wave incidents on a surface perpendicular to the propagation direction and is completely absorbed, the *radiation pressure* is calculated as (Francis, Baker et al. 1998)

$$p_{rad} = \frac{p_0^2}{2\rho_0 c^2} = \frac{I}{c} \qquad (2)$$

where p_0 is the acoustic wave amplitude, ρ_0 the fluid density, c the speed of sound and I the intensity of the wave. This *radiation pressure* is written in units of *Pascals* (Pa), but it determines the *radiation force* per unit area (N/m^2) that the surface experiences by the wave. In reality the wave will not be totally absorbed, therefore the *radiation pressure* depends on the surface material properties, i.e. its reflection and absorption coefficient and its geometry.

Nyborg very well documents the nonlinear phenomenon acoustic streaming in several publications. For very low-pressure amplitude the propagation of ultrasound can be treated by a first-order equation (Wu and Nyborg 2008). For higher amplitudes the equation becomes non-linear and the wave propagation cannot be treated as a first-order phenomenon anymore. Using second-order approximations Nyborg (1965) solved the *Navier-Stokes equation* and explained acoustic streaming. Acoustic streaming occurs in high-intensity sound fields where the sound waves generate circulatory mean

mass flow. The effect is associated with the friction between a vibrating medium in contact with solid surfaces.

It is mentionable that the *mechanical index* (MI)

$$MI = \frac{PNP}{\sqrt{f}} \quad (3)$$

where *PNP* is the *peak negative pressure* and *f* is the ultrasound frequency, estimates the likelihood of the onset of *cavitation* or any other mechanical effect. It is for example highly improbable that *cavitation* will occur if the mechanical index is below 0.7 (Hoskins, Martin et al. 2010).

2.3 Cavitation

A few non-linear mechanical effects of ultrasound were already mentioned in 2.2.2. However, *cavitation* demands more attention due to its major influence on any sound field.

2.3.1 Mechanism

Changes in local pressure within a liquid cause the formation and growth of gas- or vapour-filled bubbles. These very small (few nanometers) bodies also known as cavities might

> *expand and contract according to the varying ambient pressure as a result of the compressibility of the gas they contain* (Frenkel 2010).

In contrast to all effects mentioned previously, *cavitation* is caused by such bubble activities. Initially bubble formation requires a pre-existence of "*cavitation* nuclei", small gaseous bodies (Coakley and Nyborg 1978), which are alternately compressed and expanded during a sonic cycle, whereas they will experience positive pressure if they are compressed and *negative pressure* if they expand due to mechanical tension. *Negative pressure* (in literature often termed *rarefactional pressure*), i.e. when the ambient pressure is above the one of the local pressure of the wave, leads to diffusion of gas into the bubble, thereby enlarging it. On the contrary during compression only small amount of gas is leaving the bubble. As a consequence in case of positive bubble growth, gas inflow has to be greater than the outflow (Frenkel 2010).

This kind of diffusion is known as “rectified diffusion” and is discussed in detail in Hsieh and Plesset (1961).

2.3.1.a Cavitation threshold

The extent of *cavitation* and at which time a sound field gives rise to *cavitation*, depends on

> *the size of the nuclei, ambient pressure, amount of dissolved gases, vapor pressure, viscosity, surface tension and the frequency and duration of the insonication* (Ensminger and Bond 2011).

2.3.1.b Bubble Growth

In today’s research, *cavitation* is separated into *stable* and *inertial cavitation* (2.3.2). The underlying reason for these two types of *cavitation* is the different bubble activity due to the driving parameter, *the negative pressure*. The *Rayleigh-Plesset equation*

$$\rho\left[RR'' + \frac{3}{2}R'^{2}\right] = [p_v - p_\infty(t)] + p_{gO}\left(\frac{R_0}{R}\right)^{3k} - \frac{2S}{R} - 4\mu\frac{R'}{R} \qquad (4)$$

characterizes the activity of a single bubble by calculating its change in radius when set under pressure. The form of the bubble is assumed to remain spherical for the bubbles lifetime. Within this equation we find the first and second order derivatives with respect to time of the bubble radius R (i.e. R' and R''). The term p_v-$p_\infty(t)$ calculates the difference between the pressure inside (p_v) the bubble and the pressure over time from far outside $p_\infty(t)$ the bubble. In order to solve the equation the liquid is assumed to be infinite. The second term on the right side, where p_{g0} is the instantaneous partial pressure of the gas inside the bubble, shows the polytropic behavior, i.e. the non-condensability, of the gas inside the bubble, whereas the mass is assumed to remain constant. The polytropic coefficient k characterizes the thermodynamic behavior of the gas. If $k = 1$ the bubble temperature is constant, in the case of $k = \gamma$ (heat capacity of the enclosed gas), the system is adiabatic. Furthermore, the surface tension coefficient S of the bubble is included in the *Rayleigh-Plesset equation.* This physical quantity is usually given in N/m. In the last term the viscosity μ of the liquid is taken into account (Franc 2007).

2.3.2 Stable and Inertial Cavitation

The distinction between *stable* and *inertial cavitation* is based on the different behavior of bubbles. Stable *cavitation* occurs when the gas bubbles in the ultrasound field oscillate (i.e. increase and decrease) in radius in a periodic and relatively permanent way over a longer time. This oscillation is referred to as *stable*, hence in this case *cavitation* is termed *stable cavitation* (Ensminger and Bond 2011). In contrary to that during *inertial cavitation* bubbles increase their radius during short ultrasound pulses of high acoustic pressure (through rectified diffusion) to the extent where the pressure exceeds a threshold and the bubbles collapse violently. As *cavitation* only occurs above this threshold it is characteristic for *inertial cavitation*. The phenomenon is mainly accelerated by the mass (i.e. the "inertia") of the liquid that surrounds the bubbles (this explains why it is termed *inertial cavitation*) (Hoskins, Martin et al. 2010). Note that the energy dissipation due to the fragmentation of the bubble is very high. Several underlying factors that determine the energy dissipation such as viscosity or thermal conduction are listed in Tunc and Delale (2003).

The resulting shear stress by the onset of both *cavitation* types may cause the disruption of cell junctions. These phenomena are also accompanied by extreme temperature rise (up to 7200°C (Ensminger and Bond 2011)) and by very high acoustic pressure (up to 520 MPa (Ensminger and Bond 2011)). It has also been observed (Hoskins, Martin et al. 2010) that *inertial cavitation*, more specifically the collapse of the bubble, may be the reason for the formation of free radicals such as H^+ or OH^+.

2.3.3 Passive Cavitation Detection

In general *cavitation* detection can either be performed in an *active* or a *passive* mode. The listening devices used for these studies can only conduct *passive cavitation detection* (PCD) as they are just receiving transducers. On the contrary, *active cavitation detection* (ACD) requires two transducers - one that sends out an acoustic wave toward the region where *cavitation* should be detected while the other one operates as an element that receives acoustic reflections of the bubbles. According to Salgaonkar, Datta et al. (2009), Ashokkumar, Hodnett et al. (2007), Husseini, Diaz de la Rosa et al. (2005) (to mention just a few) clear signs of *cavitation* can be found in the acoustic emission spectrum (amplitude over frequency) acquired by a listening device (i.e. hydrophone). As it will be shown several ways to quantify a *cavitation* event exist, but it is a fact that non-linear

bubble oscillation (which is an strongly related to *stable cavitation*) cause subharmonic and ultraharmonic emissions that are visible in the frequency spectrum.

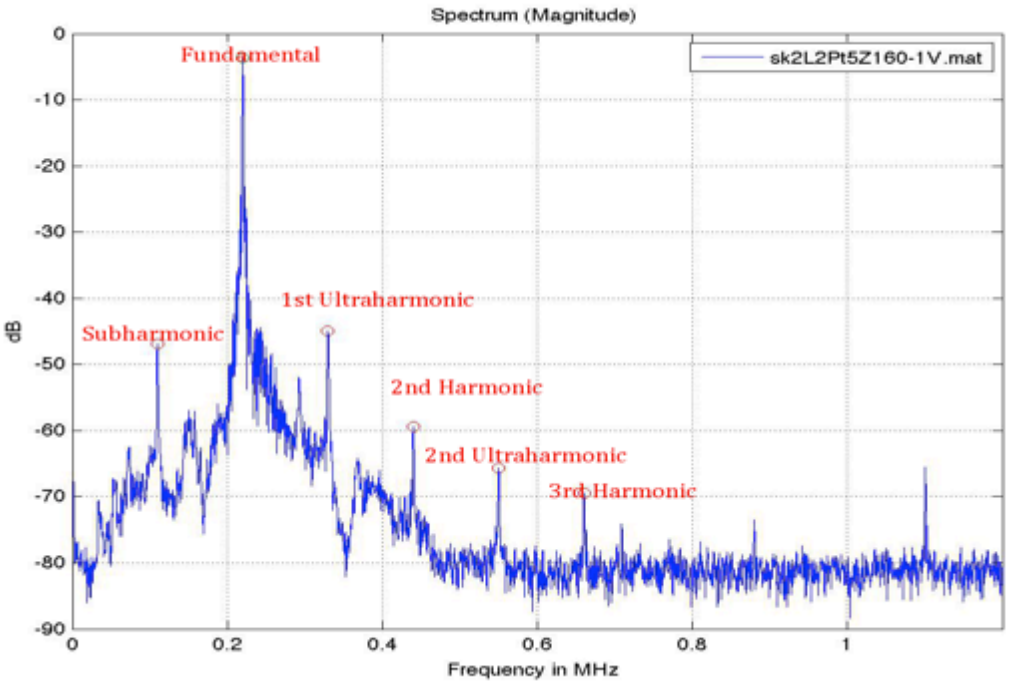

Figure 8: Frequency spectrum.

Figure 8 shows an example for a frequency spectrum and the characteristic peaks for *stable cavitation*. At the transmit frequency (220 KHz) the fundamental peak is clearly outstanding. By dividing the transmit frequency by 2 we get the frequency of the so called subharmonic (110 KHz). Furthermore, the 1st and 2nd harmonic

$$frequency\ of\ n^{th}\ harmonic = n \times frequency\ of\ fundamental \qquad (5)$$

where n =1,2 and the 1st and 2nd ultraharmonic

$$frequency\ of\ n^{th}\ ultraharmonic = \frac{(2n+1) \times frequency\ of\ fundamental}{2} \qquad (6)$$

where n =1, 2 , are visible in Figure 8. In literature an indication for *inertial cavitation* is a significant rise of the "broadband signal". *Cavitation* measurements within this thesis focus on the detection of *stable cavitation*.

2.3.4 Evaluation of the Frequency Spectra

It is explained in 2.3.3 that *cavitation* can be identified by certain features of the spectral content. Nevertheless, there is no unique way to quantify *cavitation* and to determine its threshold. Based on a thorough literature review a method was defined to quantify *cavitation* or more specific the spectral content of the generated spectra such that when this quantity exceeds some defined reference level (threshold) *stable cavitation* occurs. *Cavitation* detection mainly depends on the limitation of the instrumentation (background noise level) and the interpretation of the acquired signals. Therefore it sometimes may not be detected although already present. The following section should show examples of approaches to interpret the frequency spectra. Within the studies for this thesis we basically measure a voltage signal but the threshold can be expressed as different physical quantities such as intensity, or PNP.

A possible way quantifying *cavitation* is to calculate

> *the definite integral of the squared acoustic response between two frequencies, f_1 and f_2,*
>
> $$energy = \int_{f1}^{f2} V_C\,(f)^2 df \qquad (7)$$
>
> *where $V_C(f)$ is the magnitude of voltage signal acquired with the hydrophone at frequency f* (Ashokkumar, Hodnett et al. 2007).

In other words, we would have to integrate our acoustic spectra in a certain frequency range and determine a threshold by comparing this value to a reference. This approach was considered as unsuitable since the authors did not elaborate any method that defines a threshold. According to Bader and Holland (2012) a *cavitation* event is quantified by the difference in amplitude of pressure (in dB) between the fundamental and the subharmonic. If this difference is less than 20dB, *cavitation* occurs. Another reasonable approach reported by Farny, Holt et al. (2008) could be used to quantify *cavitation*. In this case the threshold would be defined by three standard deviations above the mean background signal. This would of course include choosing an appropriate background signal. After careful deliberation a slightly modified method by Farny, Holt et al. (2008) seemed convenient for the performed research as a threshold could be easily defined and compared to the spectral content.

2.3.5 The Role of Microbubbles in causing Cavitation

Using MB as contrast agents is already very promising method in diagnostic imaging with ultrasound. Beside that field of application, research focuses more and more on the contribution of MB to therapeutic applications. In literature (Wu and Nyborg 2008), free bubbles are distinguished from encapsulated MB (EMB). The difference between these two types is that free bubbles tend to dissolve rapidly due to their instable shell structure. In general these free bubbles are cavities filled with air, other gases, or gas vapor from surrounding liquid. Free bubbles usually have a short lifetime since either gravitational force or the so called *"Laplace pressure imbalance"* causes them to dissolve. On the other hand they might grow as explained in 2.3.1.b. However, the application of bubbles as for example contrast agents requires a technique that encapsulates the bubbles by either lipid or proteins with the main goal to stabilize the boundaries of these free bubbles and to prevent leakage of air or gas (e.g. EMB filled with inert gas such as perfluorocarbon).

Cavitation events usually occur at high negative acoustic pressure without any supporting agents. As shown in this thesis and documented by Dijkmans, Juffermans et al. (2004) the combination of FUS and MB lower the threshold for *cavitation*. As a consequence less pressure is needed to cause *cavitation*, which also means that the body is exposed to lower acoustic pressure.

2.4 Treatment Envelope

Due to the novelty of the research field, the *treatment envelope* (TE) has yet to be defined by standard terms. In general the boundaries of this specific volume within the skull should represent the limit for therapeutic applications of FUS. Defining the TE contributes to the sound field characterization, which is crucial when applying FUS. Scattering, absorption, reflection by the skull bone are processes that mainly influence the sound field configuration in the brain.

Beside the necessity and importance for the following *cavitation* studies to have the TE well defined, previous studies by the Focused Ultrasound Foundation aroused our interest in evaluating the TE to explore the underlying acoustic reason for the thermal effect. If the correlation between the focal zone with skull heating is evaluated correctly this could be of great benefit to several non-invasive surgical applications in the brain.

As shown in 2.2.2 therapy by ultrasound can either be thermal or mechanical. In literature Merz (2002), Hoskins, Martin et al. (2010) et al. terms like power, energy and intensity are related to the thermal type of therapy. On the other hand, *cavitation* (the most important mechanical effect induced by ultrasound) is in particular determined by the PNP of the sound. It is therefore reasonable to separate a *"thermal-therapy"* TE from a *"mechanical-therapy"* TE. Note that the intensity is proportional to the square of the PNP (Baron, Aubry et al. 2009). This fact implicates that the *"mechanical-therapy"* TE is larger than the *"thermal-therapy"* TE. Within this thesis both the *"thermal-therapy"* and the *"mechanical-therapy"* TE are determined. The way in which we defined the boundaries of the TE is documented in the methods part (3.5.1).

3 Methodology

3.1 Research objects

3.1.1 Human Cadaver Skulls

The measurements required a set of two full human cadaver skull specimens (Figure 9 and 10). They were obtained from the UCSD Medical School Division of Anatomy, but no further background information was provided. For identification numerical values were assigned (*Skull 1* and *Skull 2*).

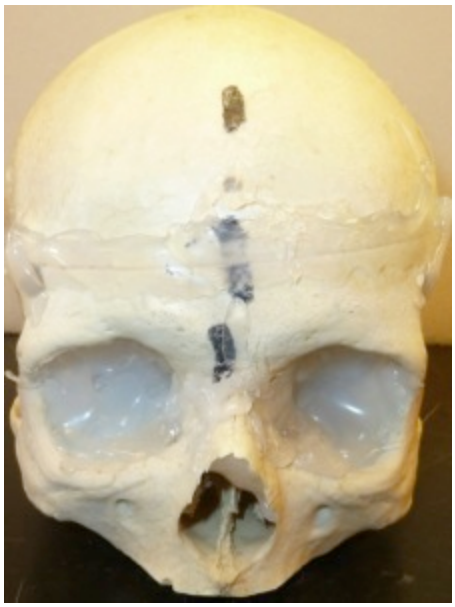

Figure 9: *Skull 1*. Frontal view.

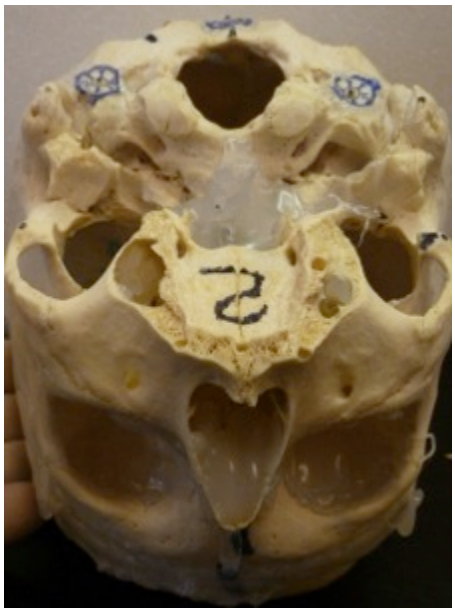

Figure 10: *Skull 2*. Frontal view, upside down, no plugs.

The cleaned skulls were stored in a dry state. Preparation of each skull prior to the measurements included the drilling of four holes by a trephine drill. The holes, which had a diameter of 2 cm in the transverse plane, were located around the foramen magnum. The cylindrical low-cut bone pieces (referred to as plugs) were glued back into their original position as desired (Figure 11). The ulterior motive for that was to examine whether the plugs had an effect on the acoustic field distribution or not. Due to the guide-bit of the trephine drill a 4 mm hole in the center of each plug could be used to insert the hydrophone for uniaxial (z-direction) measurements. Figure 9 shows *Skull 1* in the dry state in a frontal view. Figure 10 is a picture of *Skull 2* as it looks like upside down. Note that two of the four holes are visible next to the maxillar bone.

A coordinate transformation between the CT and the FUS frames of reference required the definition of at least 3 fiducial points on the skull itself. At the beginning, for *Skull 1*, the center of each plug was used as fiducial point but due to the insufficient accuracy new fiducial points were defined later on. In case of *Skull 2* radio-opaque markers were glued to three positions on the skull. All these points allowed it to replace the skull when desired, without loss of spatial registration. Furthermore, they were necessary to reconstruct the skull within a computer simulation. The fiducial points for *Skull 2* are shown in Figure 12 as an example.

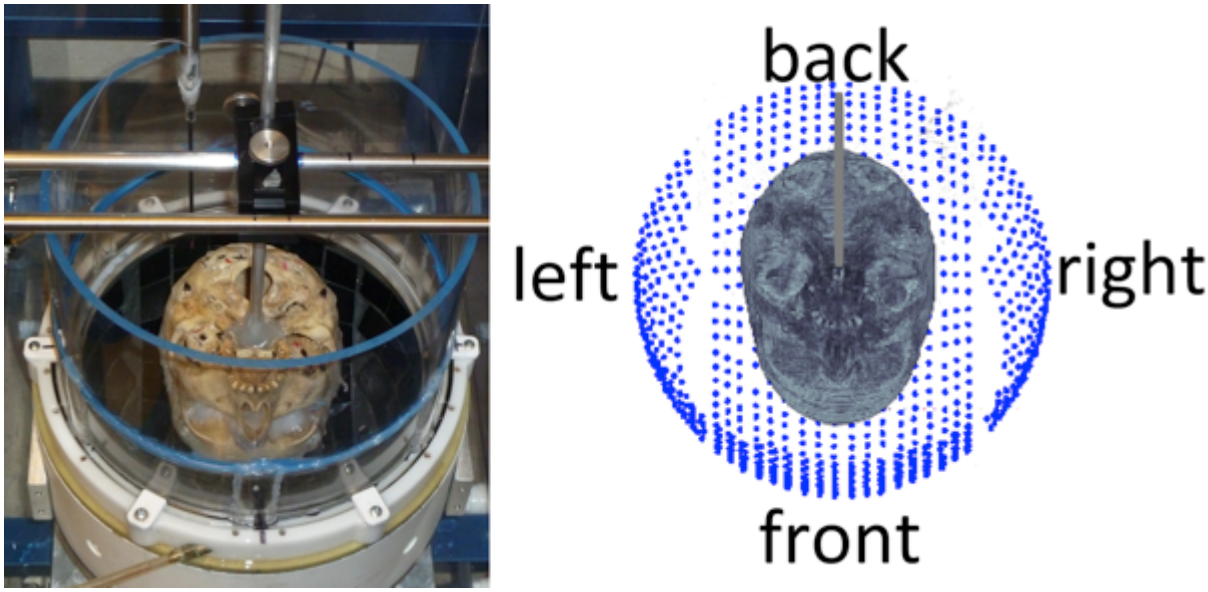

Figure 11: Positioning of the skull within the transducer (view: front/top). Note that in this figure all plugs are glued in. The blue dots represent the transducer elements. In some areas are no elements (white gaps).

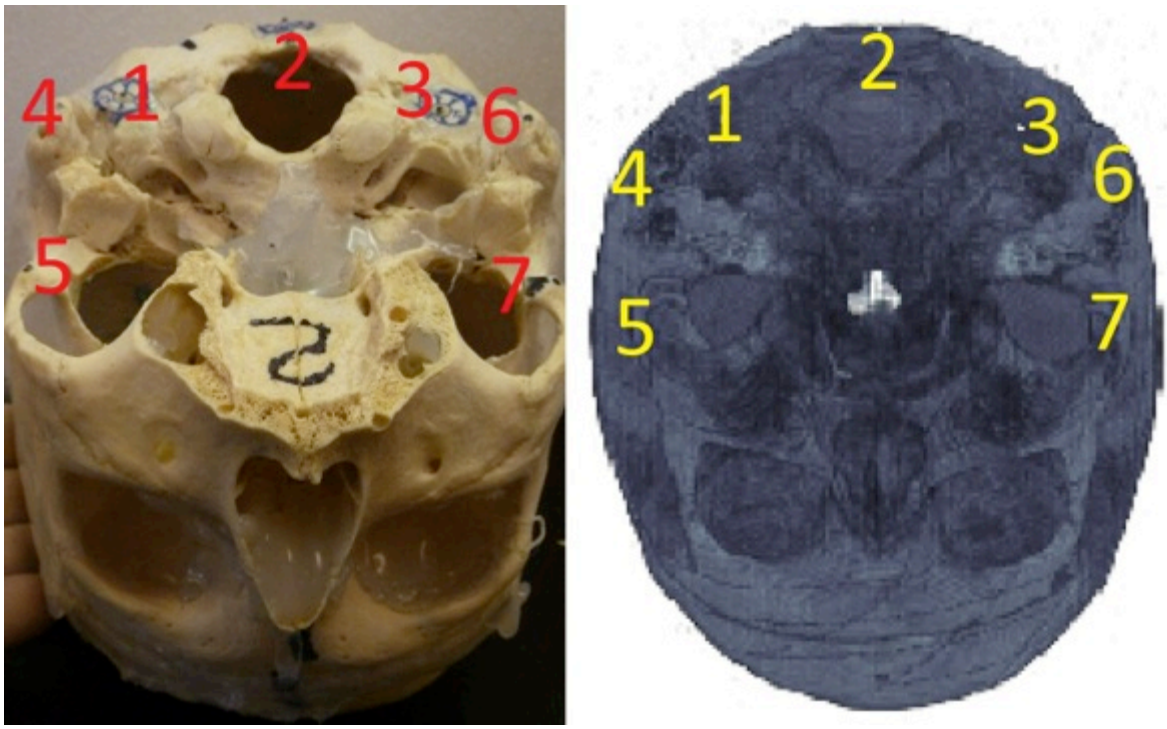

Figure 12: Positions of the fiducial points on *Skull 2* (view: front/top). On the left side the 3 radio-opaque marker can be seen (Point 1-3).

For the following *cavitation* studies, on *Skull 1*, two additional holes were drilled, the one in the forehead, the other one in the back of the head, both in the calvarium. These holes were used to attach and position a tube, which had to run through the skull. The TE studies were performed on both skulls, whereas only *Skull 1* was used in the *cavitation* studies with the tube.

3.2 Research Instruments

3.2.1 Focused Ultrasound System

For all experiments the ExAblate™ 4000 (InSightec Inc., Tirat Carmel/Israel) was used. The key component of this FUS device is a headsystem where multi-channel high-powered phased array transducers are placed in a hemispheric arrangement of 30 cm in diameter (www.insightec.com). In total 973 active piezo elements can be operated independently. This helmet-like application is connected to a computer where different operating parameters are selected and insonation is controlled. The transmit frequency of the ExAblate™ is preset to 220 kHz and cannot be changed by the user. For the sake of simplicity the headsystem will be referred to as transducer in this thesis. Furthermore, it has to be mentioned that ExAblate™ is used as an interchangeable term for the FUS system.

The transducer is capable of generating a sharp focus (radius: 2.0 mm in x-,y- and 3.0 mm in z-direction). Of great benefit for this research is the possibility to steer the focus electronically from the center of the transducer in a radius of 3.0 cm in any direction without loosing its shape. Due to the hemispheric arrangement the target is insonated from all around.

3.2.2 MATLAB

For the entire simulations, data analysis and storage management MATLAB 2012b (The MathWorks, Inc.), Version 8.0 (for Macintosh) was used. Due to the analysis of large datasets a 64-bit version became inevitable.

3.2.3 Acoustic Intensity Measurements System

AIMS (Acoustic Intensity Measurement System, ONDA, Inc., USA) Vers.4.2 controlled the movement and positioning of the hydrophone. Waveform data was collected and saved in a text format. The software allows generating 1-, 2-, or 3-dimensional acoustic field scans, whereas a 3D scan is practically a stack of 2D scans. AIMS was installed on a Windows-XP platform. The operating computer is referred to as AIMS computer.

Automated Scanning Tank

The 0.89 m X 0.51 m X 0.58 m acrylic wet-tank of the AIMS satisfied the requirements for the measurements. The tank was empty, the transducer placed inside of it. The large viewing area of the tank made it possible to have full view of the transducer. A motion unit is positioned on the rim of the tank. Figure 13 shows the transducer placed in the wet-tank and the coordinate system of the motion unit.

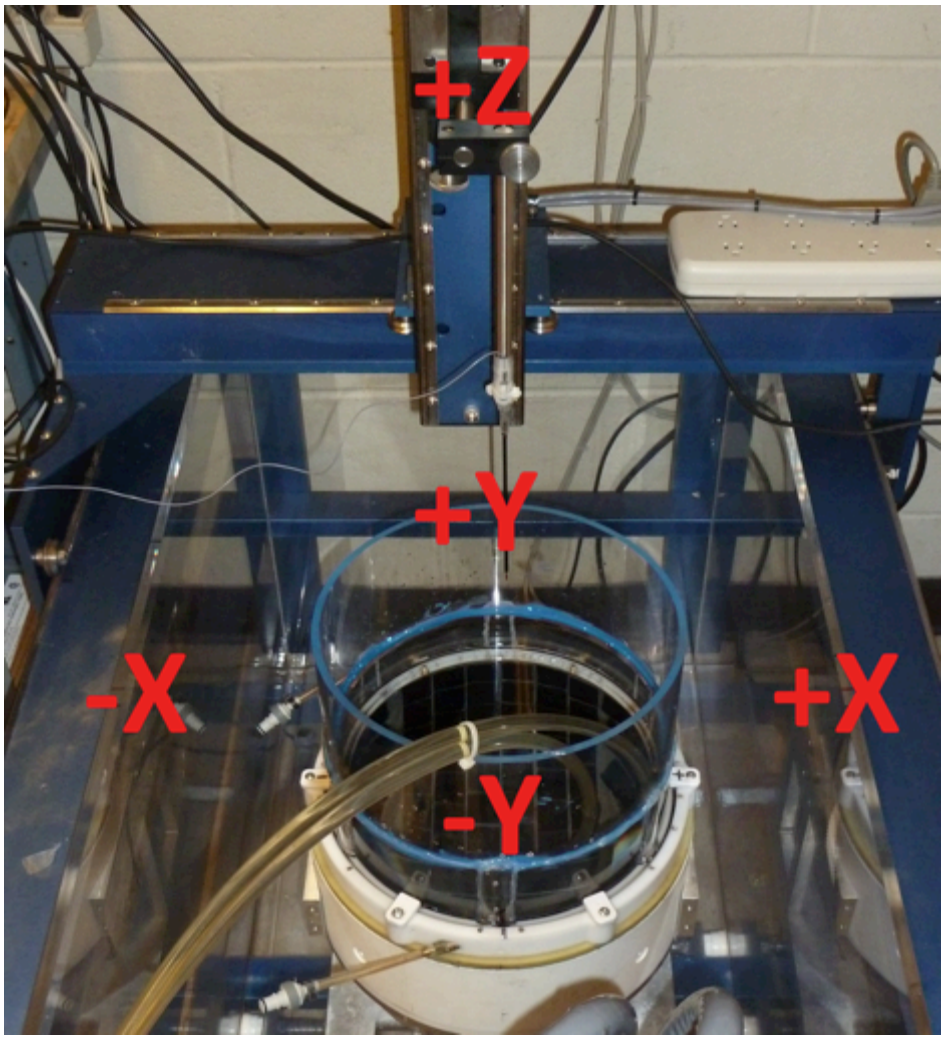

Figure 13: Automated scanning tank. The transducer system is positioned in the center. The coordinate system of the motion unit and measurements: positive x (+x) points towards the right wall of the tank, negative x (-x) in the opposite direction, positive y (+y) points towards the back wall, negative y (-y) in the opposite direction, positive z (+z) upwards, negative z (-z) towards the ground.

Motion Unit

The position of the hydrophone was changed with the stepper motors of the positioning system. A unidirectional step had the length of 1 mm for all the measurements, a smaller size has been considered as redundant due to the 0.8 mm diameter of the hydrophone sensing element. The motion unit allowed the movement in x-, y-, and z-direction and was controlled by AIMS.

3.2.3.a for Treatment Envelope Studies

Before a single scan the outer limits (mm) of the scan had to be set in the AIMS software. Within the range spanned by these limits the hydrophone would move in increments (mm) of size defined by the user. For each resulting step the hydrophone acquired a series of waveforms. For data storage management one folder per scan has been created

prior to the scan. The identity of the scan was incorporated into the name of the folder, and within this folder a root file with all the scan settings was named.

3.2.3.b for Cavitation Studies

Experiments focused on *cavitation* research did not require any set up of the AIMS software. The motion unit was only used to move the hydrophone as a pointer that identifies 3D spatial coordinates.

3.2.4 Listening devices

3.2.4.a for Treatment Envelope

To measure the acoustic field within the TE studies the hydrophone (Model Y120 from Sonic Concepts Bothell, WA, USA) was mounted to the end of 38 cm stainless steel shaft. The frequency range of this hydrophone covers a range from 50 kHz to 1.9 Mhz. The active element with a diameter of 0.8 mm is protected by a ceramic covering and designed for operation in a high-pressure field. After the positioning and calibration of the hydrophone tip it could be used as pointer that determines the spatial location as well (Figure 14). This was necessary if the skull had to be translated or repositioned in order to maintain the accuracy of spatial registration.

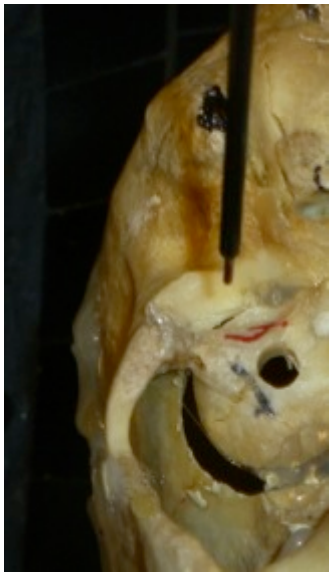

Figure 14: Tip of the hydrophone. One glued plug with its small center hole can be seen.

3.2.4.b For Cavitation Studies

For the *cavitation* studies we used a PCD sensor provided by the FUS manufacturer. The PCD sensor was essentially the same as any of the transducer elements, i.e. a piezoelectric crystal with a single frontal matching layer, air backed, undamped, and repurposed as a receiver element. This sensor was glued to the transducer and aimed to the focus at x = 0 mm, y = 0 mm, z = 150 mm and had a frequency sensitivity range of 75 kHz to 500 kHz.

3.2.5 Oscilloscope

Waveforms (voltage) were captured with the digital storage oscilloscope (DS05012A from Agilent Technologies Colorado Springs, CO, USA), having the hydrophone plugged in to the channel 1 input. A function generator was connected to the external trigger input.

3.2.6 Function Generator

A function generator (Agilent 3320A, Agilent Technologies, Loveland, CO, USA) was used to trigger the ExAblate™ and the oscilloscope externally.

3.2.7 X-Ray Computed Tomography Scan

Skulls were scanned with a 64-slice CT system (Discovery CT750 HD GE Medical Systems, Waukesha, WI, USA). The CT scanner is located in the Hillcrest Medical Center, San Diego. The skulls within the vacuum chamber were scanned to create a set of transverse images. The resolution per image was 512 X 512 pixels, covering 320 mm X 320 for pixel dimensions of 0.625 mm. Each slice had a thickness of 0.625 mm, which in total sums up to a set of 0.625 mm cubic voxels. The scans were done in a helical mode, a tube voltage of 120 peak kilovoltage (kVp), with a boneplus reconstruction kernel. This feature of the scanner software enhances bone edges and details. All the data was stored on a compact disc in DICOM format and imported by Osirix, which was used for reconstruction of the skull in MATLAB.

For visualization the CT data was imported into MATLAB, where the data had to be converted to Hounsfield Units (HU). HU are defined as

$$HU = 1000 \times \frac{\mu - \mu_W}{\mu_W} \quad (8)$$

where μ is the linear attenuation coefficient of the image pixel before conversion and μ_W the attenuation coefficient of water (Bushberg, Seibert et al. 2001). Water is known to have an attenuation of 0 Hounsfield while -1000 HU are assigned to air.

Rescale values stored in the DICOM metafiles were used for the conversion - more specific two values, the rescale slope (= 1) and the rescale intercept (= -1024), allowed to transform pixel values to HU by a simple subtraction of 1024 from the CT values.

3.3 Research Design

The oscilloscope as well as the motion unit was connected via USB to the AIMS computer. The hydrophone was plugged in to the channel 1 input of the oscilloscope. The function generator triggered both the ExAblate™ and the oscilloscope externally. A remote control of the ExAblate™ with the AIMS computer was established in order to control all the settings from a single system. The transducer was positioned in the empty wet-tank under the motion unit. Acoustic waves were acquired by the hydrophone and the collected voltage signal was digitized with the oscilloscope. Furthermore, AIMS captured the signal of the oscilloscope. An overview of the set-up is shown in Figure 15.

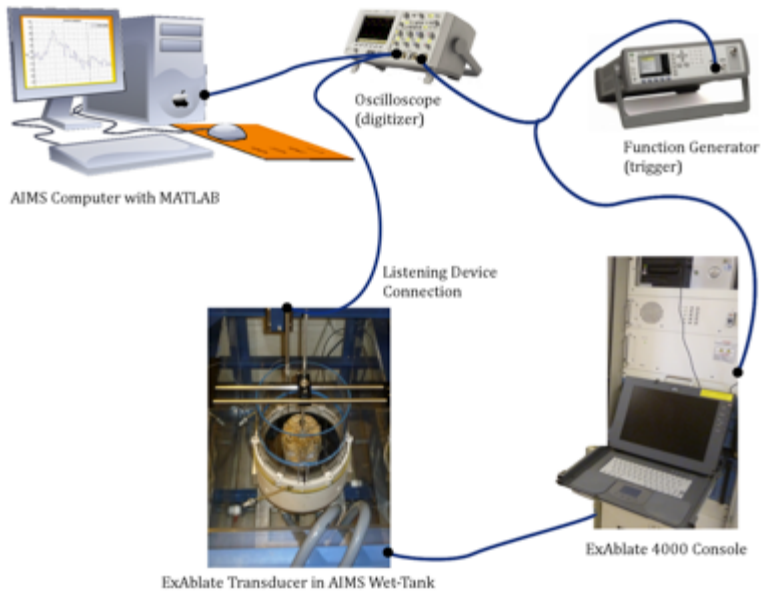

Figure 15: Schematic view of the set-up.

3.3.1 Fixture

For degassing and the CT scan each of the skulls were attached to acrylic stereotactic fixture. Note that the fiducial points on the skull were determined in the dry state of the

skull, i.e. before degassing and the CT scan. However, after the CT scan the fixture was removed and a metal rod was attached to a point forward of the foramen magnum and between the lower two access holes. That set-up provided the necessary freedom for movements in x-, y- and z-direction. The metal screw that served as an attachment point for the rod remained in the skull during the scan. Possible artifacts due to the screw were filtered within the reconstruction algorithm in MATLAB. A modified standoff was constructed for the transducer so that the skulls would remain immersed in degassed, deionized water when raised to the higher z-levels.

3.3.2 MATLAB Simulation

3.3.2.a for Treatment Envelope Studies

The complexity of the measurements owing to the combination of electronic and mechanical steering required a simulation of the measurement steps. To simplify the data acquisition a MATLAB code was written that calculated the position of the acoustic focus (accomplished by electronic steering) at a certain translation of the skull (mechanical steering).

3.3.2.b for Cavitation Studies

Based on the data derived from the TE measurements a simulation in MATLAB calculated the positioning of the tubing.

3.3.3 Electronic and Mechanical Steering

Due to the limitation in beam steering (electronic steering) of the FUS system the natural focus could not be set to the desired points. To cope with this problem an additional steering technique, i.e. mechanical steering, was used. Instead of remaining the skull at one position within the transducer, it was translated manually (mechanical steering), if necessary. By doing so we were able to expand the intracranial region over which acoustic measurements could be made.

3.3.4 Translation Pattern

We used different translation patterns for each skull. The reason for that was the small degree of freedom in translating the skull within the transducer without touching the transducer with the skull. As shown in Table 1 and 2 we used less mechanical steering for *Skull 2* due to its larger size. The mentioned MATLAB simulation helped to determine the ideal combination of mechanical steering and electronic steering, the first limited by

the size of the transducer, the latter limited by the FUS. Due to the different sizes of the skulls, two translation patterns were applied.

Table 1: Translation pattern of *Skull 1*.

Translation *Skull 1*		
	X	Y
Column 1	30	-30
Column 2	-30	-30
Column 3	-30	30
Column 4	30	30
Column 5	0	0

Table 2: Translation pattern of *Skull 2*.

Translation *Skull 2*		
	X	Y
Column 1	25	-15
Column 2	-25	-15
Column 3	-25	20
Column 4	25	20
Column 5	0	0

3.3.5 Measurement Positions

3.3.5.a for Treatment Envelope Studies

As previously mentioned a MATLAB code was used in order to determine the measurement steps. At each access hole in the skull base, a *measurement column* was calculated that would span the distance from the base to the apex. Numbers were assigned to each hole as shown in Figure 16. The hole in the upper left corner in the view shown in Figure 16 was designated Point 1. In clockwise manner, the holes were numbered, with the foramen magnum being Point 5. These points were located as close as possible to the centers of the access holes and could be thought of as the basal terminals of vertical lines that extended to apical points on the interior surface of the calvarium (i.e. in negative z-direction).

Holes *Skull 1* Holes *Skull 2*

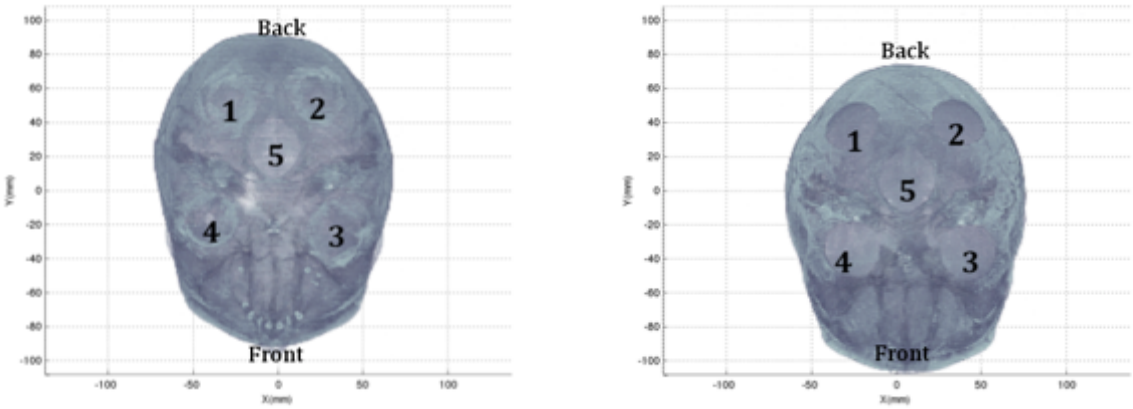

Figure 16: Measurement hole numbers (view: from base to apex) in *Skull 1* (on the left), in *Skull 2* (on the right).

Along each line we moved the acoustic focus (on the FUS) in 1 cm increments, constrained by the previously described electronic steering limit. Each focus represented the center of a 1 cm^3 *measurement cube*. A *measurement cube* was the result of a defined number of 2D scans. We basically performed 2D scans by moving the hydrophone in 1 mm steps. 11 scans, each of them 1 cm in x- and y-direction, constituted a *measurement cube* containing 1331 measurement points. One of these cubic scans took about 12 minutes. In fact the FUS allowed us to move the focus by 30 mm in positive and negative x-, y-direction, 30 mm in positive z-direction and 29 mm in negative z-direction away from the transducers geometric focus (x = 0 mm, y = 0 mm, z = 150 mm). Bearing these limitations in mind we decided to steer electronically in positive z-direction to 180 mm and in negative z-direction to 130 mm (we could actually steer as far down as 121 mm but elected not to because we found we could span the entire *measurement column* without doing so).

In total we had 5 *measurement column*s, each of them build up by a various number of *measurement cube*s. The height of a column, or the number of *measurement cube*s per column, was first of all limited by the possible extension of electronic steering and secondly by the dimensions of the skull. It was on the one side considered as unreasonable to measure the acoustic field outside the skull and on the other side we had to avoid a collision between the scanning hydrophone and the inner skull surface. Of course we wanted to measure the greatest possible volume within the skull. To achieve that, we used the MATLAB simulation that showed we could span all these *measurement column*s using two mechanical translation points along the vertical axis (i.e. the z-axis),

referred to as *Level 1* and *Level 2*, separated by 6 cm. The middle of each segment of the *measurement column* was at the transducers geometric focus.

The order of the measurements in any column proceeds from scans near the calvarium towards to the skull base in 1 cm increments. Each *measurement cube* was defined by a level number, a column (Point) number and z-position of the FUS focus, which simultaneously represents the center of the cube (e.g. for *Z180* the z coordinate is 180 mm). Note that the *Z180* measurement for *Level 2* scans is an intracranial volume that is adjacent to the *Z130* scan of *Level 1*. Each 3D scan was interpolated from a 1 mm grid to a 0.25 mm grid to better visualize the shape of the field in subsequent reconstructions.

3.3.5.b for Cavitation Studies

The *cavitation* studies only required setting the focus to two different positions. For further information see 3.4.4.b

3.3.6 Tubing for Cavitation Studies

The desired minimal effect of the tubing on the acoustic pressure field required a special tube with a very thin wall thickness. The PE tube from Advanced Polymers, Inc. we used for the *cavitation* measurements had an inner diameter of 4.3 mm and a wall thickness of 25.4 µm. Specially for ultrasound testing, this tubing is known to have preferred acoustic properties.

3.3.7 Pump for Cavitation Studies

Sonication, especially if causing PNP values above the *cavitation* threshold, destructs MB over longer measurement periods (~1 hour). To increase the time frame and to move the MB through the tube, a peristaltic pump created a constant flow rate of 10 ml/min.

3.3.8 Microbubbles for Cavitation Studies

Beside deionized water (H_2O), BR38 MBs from Bracco (Bracco Suisse S.A., Geneva, Switzerland) were used. The behavior of the lipid-coated BR38 MBs was known from other previous studies, e.g. by Petit, Gaud et al. (2012). For the *cavitation* studies 5 ml BR38 were added to 500 ml of deionized water and prior to application the solution was mixed for 5 minutes with a magnetic stirrer.

3.4 Data Acquisition

In contrary to prevent *cavitation* during the TE measurements, the aim for the *cavitation* measurements was to cause *cavitation*. These two desired effects occasionally required different instruments settings (3.4.4, 3.4.5, 3.4.6, 3.4.7).

Extensive studies were made on *Skull 1* prior to taking TE data to determine 1) the effect with and without turning off the transmitter elements in front of the eyes (see 3.4.2) and 2) the effect of making measurements with and without plugs in place (see 3.4.3).

3.4.1 Degassing

A custom-made acrylic vacuum chamber was filled with deionized water, sealed, and placed under house vacuum (-300 mm Hg). The skulls were degassed in this chamber for at least three days prior to the CT scans to ensure proper degassing. According to Pichardo, Sin et al. (2011) negative vacuum pressures are required if the degassing duration is shorter. White, Clement et al. (2006) proved that sound speed through bone specimen changes a small but statistically significant amount due to its desiccation and rehydration. Since several previous serial studies on these skulls did not exhibit any changes in acoustic measurements, we assumed changes to the acoustic properties over time due to desiccation or rehydration to be negligible.

All the measurements called for degassed deionized water in the transducer. The water was degassed to less than 2 parts per million dissolved oxygen as measured by color-change test vials and was deionized to less than 0.05 microsiemens conductivity with a laboratory water filtration/purification system.

3.4.2 Acoustic Correction Table

According to the simulation a significant number of elements might transmit through the eye sockets when the skulls were at *Level 1*. By ray tracing we were able to identify these elements of the transducer that might contribute to distortion in the focus and introduce measurement artifacts. Afterwards we created an acoustic correction table (ACT) and loaded this table into the FUS transmission control software in order to turn off the elements in front of the eyes (Figure 17). Finally we measured the effect on the focus to determine whether the ACT was necessary.

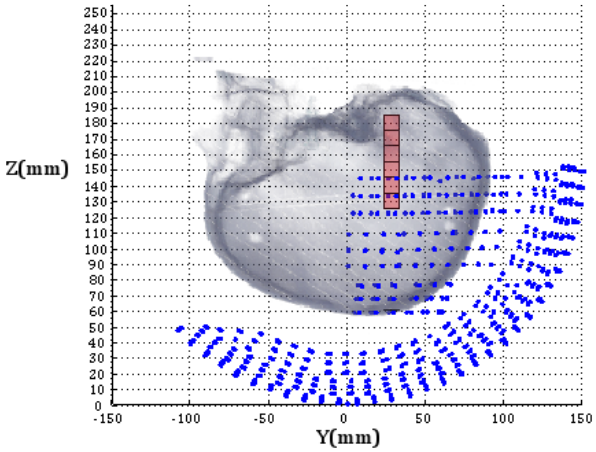

Figure 17: Elements (blue dots) turned off by the acoustic correction table (view: from right side). Active elements are blue dots.

3.4.3 Plugs

Uniaxial scans (z-direction) with and without plugs in place were performed to address our concerns whether the plugs have an effect on the acoustic field being measured by the following 3D scans in the *measurement column*s. For the first scan with all plugs glued in (Figure 18) we guided the hydrophone through the center of one plug in order to take the measurement on the z-axis, continuing at the same position but without the one plug in place. In the following we moved the hydrophone to the center of the next plug and repeated the uniaxial scan with and without that plug glued in. We performed scans for the two remaining positions in the same manner until all the plugs were removed.

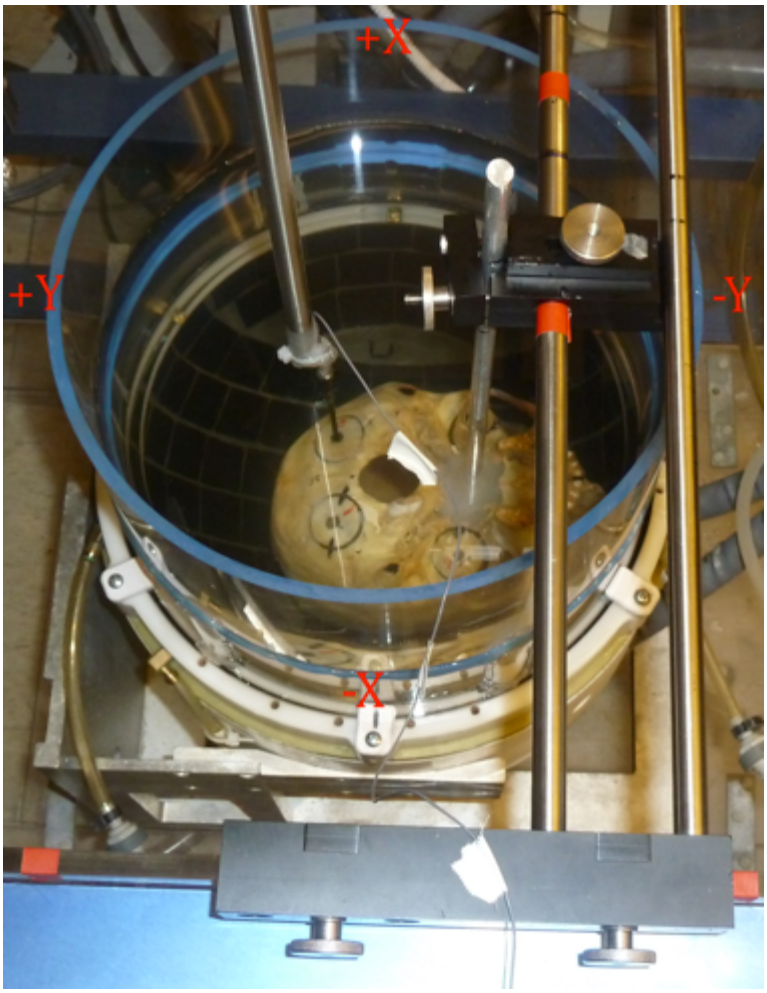

Figure 18: Uniaxial scan with all plugs in place. The hydrophone is guided through the small hole at point 2 (Column 2).

3.4.4 FUS Setting

3.4.4.a for Treatment Envelope Studies

In order to define the TE we used 14.5 Watts (W) regular sonication power (electric power) in order to achieve that 10 W of acoustic power are transmitted by the transducer elements into the medium. Beside some exceptions, in this thesis acoustic power is given. Measurements without a skull in the transducer at an acoustic power of 10 W showed no *cavitation* events. Yet the signal with a skull in place was still strong enough to be measured. Furthermore, by awareness of the pressure caused at these power settings, it simplified the scaling process in order to evoke a certain pressure. The duration of sonication for one cube has been set to its maximum value (3000 seconds). After each scan the sonication was halted and restarted to ensure that the system did

not stop with sonication during a scan. For each cube we had to change the acoustic focus according to the MATLAB simulation.

Table 3 shows the electronic steering for each column. Note that we used a combination of electronic and mechanical steering. According to the translation pattern (Table 1 and 2) we first translated the skull and then used electronic steering to set the focus to the desired position. Z_{Start} and Z_{End} represent the center position of the lowest and the highest cube (in z-direction) for a specific *measurement column*.

Table 3: Electronic steering with the FUS after translation of the skull. "L" is the level of the skull, "Col" is the measurement column, "Z_{Start}" is the center position on the z-axis (in mm) of the lowest cube on Level L, "Z_{End}" is the center position on the z-axis (in mm) of the highest cube on Level L and x,y are the x-, y-coordinates of the focus set by the FUS.

Skull 1					
L	Col	Z_{Start}	Z_{End}	x	y
1	1	130	180	1	24
2	1	160	180	1	24
1	2	130	180	-7	25
2	2	160	180	-7	25
1	3	130	170	4	10
2	3	160	180	4	10
1	4	130	170	-10	13
2	4	150	180	-10	13
1	5	130	180	-2	28
2	5	130	180	-2	28

Skull 2					
L	Col	Z_{Start}	Z_{End}	x	y
1	1	130	170	0	21
2	1	160	180	0	21
1	2	130	170	10	25
2	2	160	180	10	25
1	3	130	170	18	-15
2	3	150	180	18	-15
1	4	130	170	-5	-15
2	4	150	180	-5	-15
1	5	130	180	6	7
2	5	130	180	6	7

3.4.4.b for Cavitation Studies

As previously mentioned, the *cavitation* studies required only two different foci. *Focus 1*, which was a point within the so called *Cube 1*, was located on *Level 2*, in *Column 4*, at x = -3 mm, y = 13 mm and z = 182 mm. *Focus 2*, which was a point within the so called *Cube 2*, was located on *Level 1*, in *Column 5*, at x = 1 mm, y = 28 mm and z = 134 mm.

Determining the threshold for *cavitation* required to sweep through different sonication power settings at the focus in *Cube 1* and *Cube 2*. Again, we used a combination of electronic and mechanical steering to move the focus to desired positions. Table 4 shows the power settings and the applied medium.

Table 4: Acoustic power [W] of the FUS in presence of MBs (Bracco 38 (BR38) or simply water (H_2O).

Cube 1	
BR38	H_2O
34.5	69
69	103.4
75.9	137.9
82.8	144.8
89.7	151.7
96.6	165.5
103.4	172.4
110.3	179.3
117.2	193.1
124.1	206.9
131	
137.9	
144.8	
151.7	
158.6	
165.5	
172.4	
206.9	

Cube 2	
Br38	H_2O
6.9	6.9
13.8	34.5
20.7	69
27.6	103.4
34.5	137.9
41.4	172.4
48.3	206.9
55.2	
62.1	
69	
82.8	
96.6	
110.3	

In all cases the function generator has triggered the ExAblate™ externally.

3.4.5 AIMS Setting

3.4.5.a for Treatment Envelope Studies

Data acquired by AIMS per measurement point comprised three acoustic parameters: *temporal average intensity* (I_{TA}), *peak positive pressure* (PPP) and PNP. Prior to each 3D scan a file on the AIMS computer had to be created where the acoustic data would be saved in. The naming of these files followed the convention pt*A*Level*B*Z*C* whereas *A* defines the hole where the hydrophone has been inserted, *B* the level of the skull and *C* the distance (mm) in z-direction from the lowest point (z = 0 mm) of the transducer to the center point of the cube. Afterwards the data has been transferred to the evaluating computer.

3.4.5.b for Cavitation Studies

The Cavitation Studies did not require any specific set up of AIMS.

3.4.6 Function Generator Setting

3.4.6.a for Treatment Envelope Studies

We used a 100 µs pulse width and a 1 % duty cycle. That means the signals period was 10 ms and each period started with a negative-edge triggered 100 µs rectangular pulse. For the following 9.9 ms of one period the signal returned to 0 V. The ExAblate™ was operated in pulsed mode and used the signal of the function generator as an external trigger input signal. Due to the transmit frequency of 220 kHz and the external trigger signal the ExAblate™ transmitted approximately 22 cycles within a 100 µs pulse.

3.4.6.b for Cavitation Studies

The function generators setting was changed to a 10 ms pulse width for the *cavitation* measurements during the application of MB. The decision to use these settings was based on an article by Howard and Zanelli (2007) et al.. According to them, a small tip of a hydrophone might represent a possible nucleation site. In order to protect the hydrophone against excessive heating or *cavitation* they recommend a short pulse width and low duty cycle. Furthermore, these settings were used successfully for previous BBB studies on mice brain where the goal was to cause *cavitation* by application of MB. A sample of the trigger signal to demonstrate the rectangular form is shown in Figure 19.

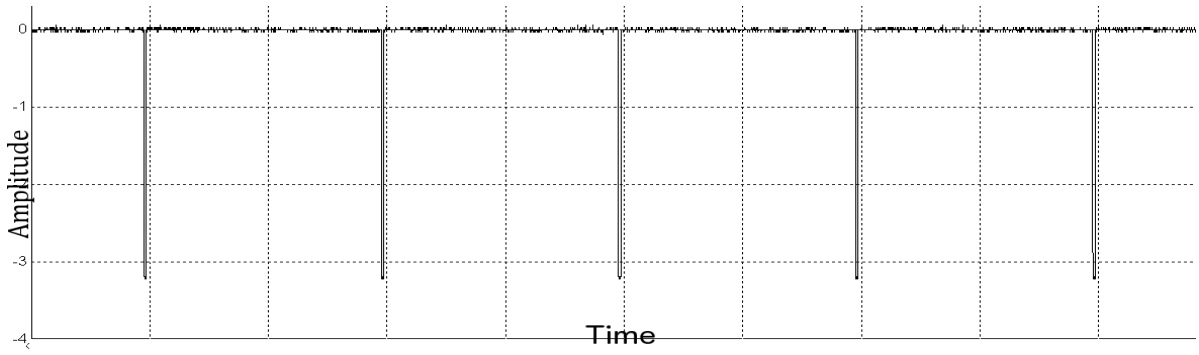

Figure 19: Rectangular trigger signal.

3.4.7 Oscilloscope Setting

3.4.7.a for Treatment Envelope Studies

The settings of the function generator determined those of the oscilloscope. For the TE measurements, the vertical scale was set to 500 mV/Div, the timebase to 20 µs/Div. Furthermore, the signal was AC coupled and a hold-off of 9.8 ms was used. The hold-off

duration was set to stabilize the signal acquisition by the oscilloscope. Basically the trigger unit ignores another trigger signal within this duration.

3.4.7.b for Cavitation Studies

Scaling for the *cavitation* studies with the MB was changed to 1 V/Div, 200 µs/Div and a hold-off of 985.7 ms. To evaluate the possible influence of the scaling on the *cavitation* measurements, a few experiments on the oscilloscope were made. We found out that the scale on the oscilloscope determines the sensitivity of the listening device. If we lowered the vertical scale the basis of the signal dropped. Lowering the scale even more would cause the basis to drop more and would let the subharmonic and ultraharmonic become visible. As the aim of all the *cavitation* measurements has been to detect *cavitation* and find a threshold, the scaling does not have an influence as long as it remains constant for all the measurements.

3.4.8 Control Data Set without Skull

To create a control data set the acoustic field without the skulls in the transducer has been measured. The data comprised measurements at the geometric focus (x = 0 mm, y = 0 mm, z = 150 mm), and at z-levels of 180, 170, 160, 150, 140, 130 mm. This control data set determined the effect on the field of electronic steering in the vertical direction away from the geometric focus.

3D scans of the acoustic intensity fields were made at the positions mentioned above. The peak intensities were at the target coordinates in all cases. The highest measured intensity was 737 mW/cm^2 at the x = 0 mm, y = 0 mm, z = 160 mm target, and the lowest was 593 mW/cm^2 at x = 0 mm, y = 0 mm, z = 180 mm.

3.4.9 MATLAB Code for acquiring Data for the Cavitation Studies

Immediately after starting the insonication with the ExAblate™ we ran a MATLAB code. That code controlled parameters of AIMS, more specifically it forced AIMS to convert the voltage signal (measured by the PCD sensor and digitized by the oscilloscope) into an acoustic parameter, i.e. pressure. Pressure was assumed to be almost proportional to the voltage signal collected by the hydrophone. However, the code instructed AIMS to acquire 10000 points for one waveform in the time domain and repopulate this dataset 8 times. The resulting matrix collected by MATLAB was a 10000 X 9-matrix, the first column showed the time data, the following 8 columns contained the waveform data.

As mentioned in 3.4.7.b for the cavitation studies the time base of the scope was set to 200 µs/Div, thus having a time window of 2 ms (10 X 200 µs = 2 ms). This implicates that with 10000 points per waveform the time increments were 0.2 µs and that with a time window of 2 ms the frequency resolution in the FFT was 500 Hz ($f_{FFT} = (2\ ms)^{-1} = 500\ Hz$). The 0.2 µs time increments set the upper frequency limit of the FFT to 2.5 MHz ($f_{FFTRange} = (0.2\ \mu s)^{-1} = 5$ MHz, frequency ranges from -2.5 MHz to +2.5 MHz).

3.5 Data Analysis

All the acoustic data was transferred to a 64-bit MAC (OS X) system for analysis and post processing. The TE was defined for *Skull 1* and *2*. For the cavitation measurements with the tube in place, only *Skull 1* was analyzed.

3.5.1 Defining the Treatment Envelopes

In order to define the boundaries of the TEs, we determined reference maxima, which were in general the highest values in intensity and PNP among all the values we have acquired for one skull. By our definition of a TE, cubes, at which the peak value (either *acoustic intensity* or PNP) was below half of its reference maximum, were considered outside of the TE. To perform an interpolation in 3D-space on the data we collected per column, the MATLAB command TriScatteredInterp seemed to be a good choice. This method uses the Delaunay Triangulation, which is of interest for the interpolation of scattered data as it connects three points nearby creating a triangle by doing that. Characteristically for the Delaunay Triangulation is that no other point lies in the circumcircle of that triangle (Figure 20 and 21). In the 3D-space the interpolated data can be seen as a composition of many tetrahedra, where the surface consists of four Delaunay triangles (Figure 22) (www.mathworks.com).

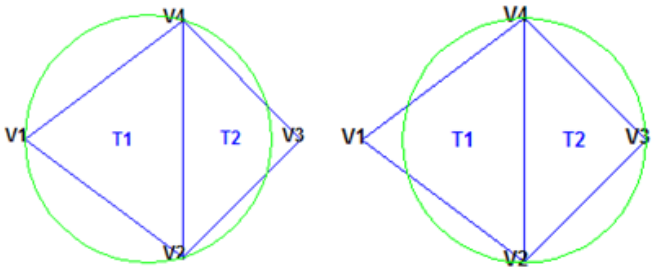

Figure 20: Delaunay triangle. No other points beside the corner points that span the triangle are located within the circumcircle of T1 (left side) or T2 (right side) (www.mathworks.com).

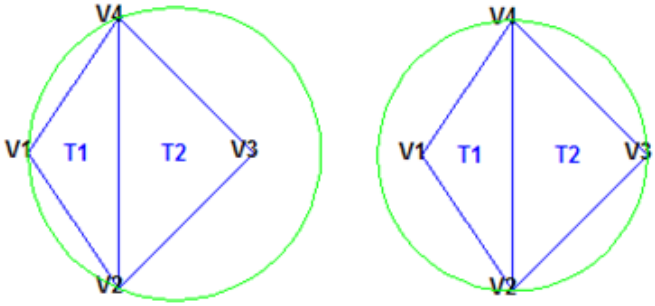

Figure 21: No Delaunay Triangle. V3 is located in the circumcircle of T1 (left side), V1 is located in the circumcircle of T2 (right side) (www.mathworks.com).

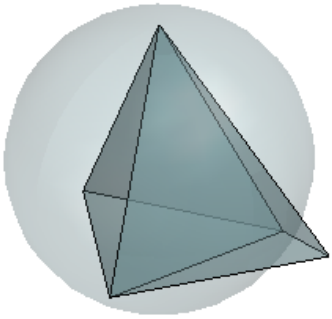

Figure 22: Delaunay Triangulation in 3D-space forms many tetrahedra. The interpolated data in this thesis can be thought as a composition of these tetrahedra (www.mathworks.com).

3.5.2 Positioning of the Tube

Finding two cubes in different columns where the difference of the maximum *peak negative pressure*s between these two cubes was more than 160 kPa required a MATLAB code. In addition to that the cubes were supposed to lie in the same Z plane, otherwise the tubing would have to be positioned in a larger angle within the skull. Unfortunately

there was no such combination, but we found one combination where the centers of the cubes were 1 cm in z-direction apart from each other. According to the simulation it was the position for the tube, which included the cube in *Level 1*, *Column 5* with its center at z = 130 mm and the cube in *Level 2*, *Column 4* with its center at z = 180 mm. Figure 23 shows the tube through the desired two cubes.

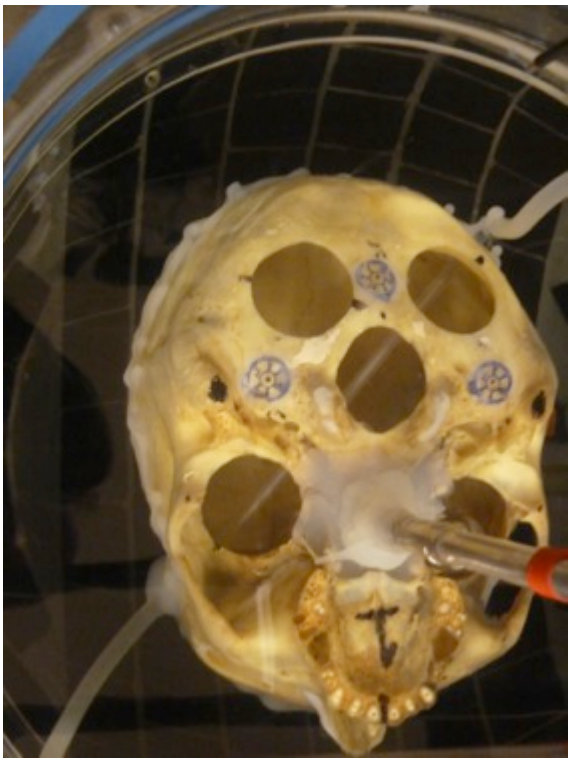

Figure 23: Tube through Column 5 and Column 3.

3.5.3 Background Signal Measurements

Analyzing the data within the *cavitation* studies required the measurement of a background signal (Figure 24). During the acquisition of this broadband signal, the FUS remained in a steady state and did not transmit. To capture all possible noise sources, the function generator and the oscilloscope operated in the way like they used to for the *cavitation* measurements.

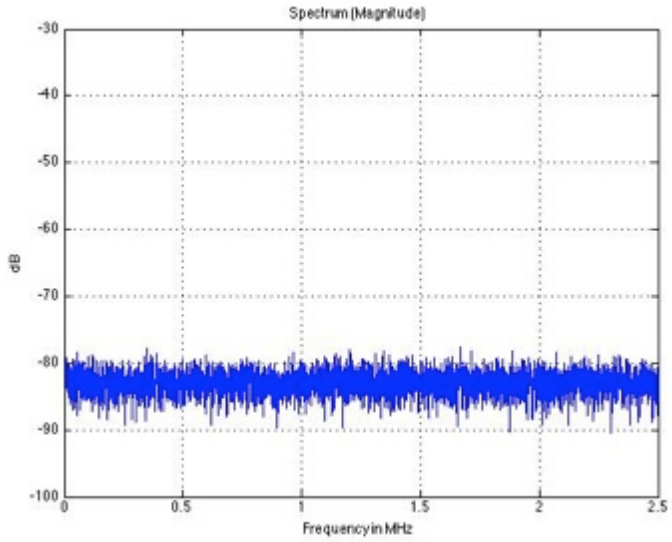

Figure 24: Example of broadband signal.

3.5.4 Preparation of the Signals for Spectral Analysis

A Hanning window was applied to the time-domain (v(t)) data to reduce the broadband leakage and bring out smaller signals. The 10000-point (n_t) time domain waveforms were zero padded to the next highest power of 2, and a 16384-point (n_{FFT}) FFT for each waveform was calculated. The resulting frequency-domain data v(f) was then averaged for each set of 8 waveforms. We then converted the frequency-domain data to the dB scale by $v(f)_{dB} = 20*\log_{10}(K)$, where K is equal to $v(f)/n_{FFT}$. For all the measurements in the current experiment only frequencies from 0 to 1.0 MHz were evaluated due to the frequency range limitation of the PCD sensing element.

3.5.5 Passive Cavitation Detection

Since no golden rule how to identify *cavitation* and to find its threshold exists, we decided to come up with a combination of the analysis method used for previous *cavitation* measurements at BURL and the one described by Farny, Holt et al. (2008). All the *cavitation* characterization was done by evaluation of the spectral components of the FFTs. This included the analysis whether *cavitation* events have been present, finding the thresholds in *peak negative pressure* for these events, and quantifying *cavitation*.

To identify *stable cavitation*, the first evaluation step comprised determining at which frequency the fundamental occurs (Figure 25). This frequency was used for calculating all other frequency values for the subharmonic, ultraharmonics, and higher harmonics. In the following the code searched for peaks in a defined range around these frequencies of interest, whereas the range was set to +/- 50 points, which means approximately +/-15 kHz. If the peak represented a local maximum as well, the

difference between the peaks amplitude and the mean value of the noise floor frequency spectrum was calculated. In case of a difference greater than 6 dB the signal at that frequency was defined as significant in presence (Figure 26).

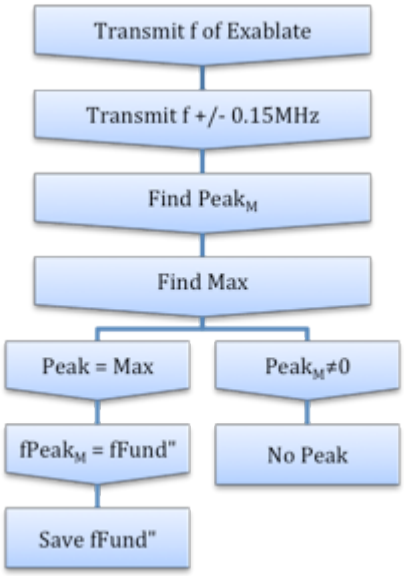

Figure 25: Workflow to determine the frequency of the fundamental.

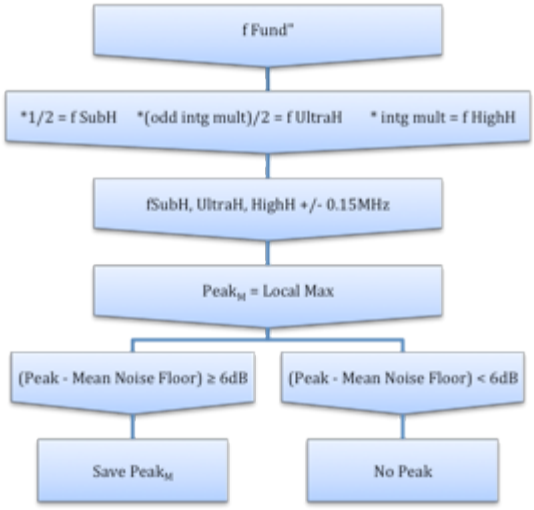

Figure 26: Workflow to determine signs that indicate *cavitation*.

Following the criteria for peaks listed above MATLAB assigned "1" for a peak satisfying all criteria and "0" else. The criteria were applied to every single spectrum providing 5 numbers (either "1" or "0" for subharmonic, 1st ultraharmonic, 2nd harmonic,

2^{nd} ultraharmonic, 3^{rd} harmonic). Again, it has to be pointed out that the MATLAB algorithm identifies *stable cavitation*, not *inertial cavitation*.

4 Results

4.1 Treatment Envelope Studies

4.1.1 Intensity and Peak Negative Pressure

Table 5 and 6 show the highest values in intensity and PNP of each cube in both skulls. The exact locations (x-, y-, z-coordinate) of these maxima are known but only needed for the calculation of the tubing path for the *cavitation* studies. Further information on the locations of the cubes is provided in 3.4.4.a. For each skull the global maximum in intensity is highlighted in red, for PNP in green. The TE boundaries are defined as the half-maximum intensity (*"thermal-therapy"* TE) or PNP (*"mechanical-therapy"* TE). Intensity or PNP measurements below this value are highlighted in yellow. The first column defines the level and the center location of the cube on the z-axis (e.g. *Z180* is the cube that has its center at z = 180 mm).

Table 5: Peak intensities and PNP for *Skull 1* from 3D scans. Unit for peak intensity is mW/cm², PNP is given in MPa.

Skull 1	**Peak Intensities From 3D scans (mW/cm²)**				
	Column 1	Column 2	Column 3	Column 4	Column 5
Level 1					
Z180	20.38	23.53			9.20
Z170	29.07	25.80	36.32	27.12	9.76
Z160	29.57	24.55	28.38	28.98	12.88
Z150	18.60	12.70	31.35	29.80	25.25
Z140	23.67	13.05	33.18	30.35	31.10
Z130	20.26	14.54	22.03	19.92	29.97
Level 2					
Z180	12.39	10.85	8.79	7.61	18.57
Z170	12.48	15.79	9.29	13.21	19.25
Z160	13.26	18.75	15.24	18.72	20.46
Z150				23.18	22.12
Z140					29.57
Z130					28.16
Skull 1	**Peak Negative Pressure From 3D Scans (MPa)**				
	Column 1	Column 2	Column 3	Column 4	Column 5
Level 1					
Z180	0.278	0.295			0.190
Z170	0.332	0.312	0.366	0.319	0.195
Z160	0.333	0.306	0.317	0.323	0.220
Z150	0.267	0.220	0.330	0.326	0.305
Z140	0.296	0.227	0.342	0.336	0.331
Z130	0.271	0.245	0.281	0.268	0.330
Level 2					
Z180	0.222	0.200	0.184	0.169	0.272
Z170	0.223	0.244	0.191	0.221	0.270
Z160	0.226	0.268	0.231	0.261	0.274
Z150				0.284	0.283
Z140					0.324
Z130					0.319

Table 6: Peak intensities and PNP for *Skull 2* from 3D scans. Unit for peak intensity is mW/cm², PNP is given in MPa.

Skull 2	**Peak Intensities From 3D scans (mW/cm²)**				
	Column 1	Column 2	Column 3	Column 4	Column 5
Level 1					
Z180					32.18
Z170	69.51	39.64	36.02	38.31	19.64
Z160	74.41	75.20	48.91	45.14	44.07
Z150	46.50	40.50	46.96	39.07	70.19
Z140	36.86	29.64	35.25	27.51	77.05
Z130	26.90	23.69	27.88	22.84	68.15
Level 2					
Z180	40.36	38.99	30.88	36.31	59.49
Z170	47.60	45.81	35.66	40.66	63.74
Z160	61.21	49.34	46.61	47.16	69.91
Z150			59.40	51.98	72.36
Z140					46.61
Z130					51.38
Skull 2	**Peak Negative Pressure From 3D Scans (MPa)**				
	Column 1	Column 2	Column 3	Column 4	Column 5
Level 1					
Z180					0.344
Z170	0.510	0.381	0.363	0.375	0.262
Z160	0.521	0.528	0.422	0.406	0.393
Z150	0.410	0.388	0.414	0.374	0.490
Z140	0.368	0.331	0.364	0.313	0.521
Z130	0.312	0.296	0.327	0.396	0.490
Level 2					
Z180	0.382	0.381	0.336	0.369	0.469
Z170	0.416	0.419	364	0.387	0.479
Z160	0.470	0.427	0.418	0.417	0.494
Z150			0.467	0.435	0.506
Z140					0.407
Z130					0.433

4.1.2 Effect of ACT

We decided against the application of the ACT due to the insignificant difference in intensity and form of the focal volume in case of both skulls if all transducer elements were either activated or a few elements in front of the eyes were not energized.

4.1.3 Effect of Plugs

The measurements performed in 3.4.3 showed that there is only a slight difference, if at all, between measurements with and without the plug in place on the active *measurement column*. The effect on the acoustic field is minimal when all of the plugs were removed. Based on that, all plugs were removed and all access holes remained unplugged during all 3D scans. That is the reason why radio opaque markers were used as fiducial points. This allowed the plugs to remain off during scanning or checking positions, which was a considerable time saver.

4.1.4 3D Plots of Scans

Different MATLAB codes can visualize the collected acoustic data in several ways. Besides the TEs, we were interested how the focal spot changes its shape at different positions in the skull. We also wanted to compare the focal volume for intensity plots with PNP plots. This can be shown in separated 3D plots of the acoustic data for each *measurement cube*. Due to the fact that in total 94 *measurement cube*s were created, only a few were plotted for demonstration purposes. Figure 27 - 32 show only sample plots of 3D plots of intensity, PNP and incident angle distribution of *Cube 1* and *Cube 2* within *Skull 1*. Note that both the intensity plots and the PNP plots are thresholded to the half-maximum for the specific scan, not the overall half-maximum.

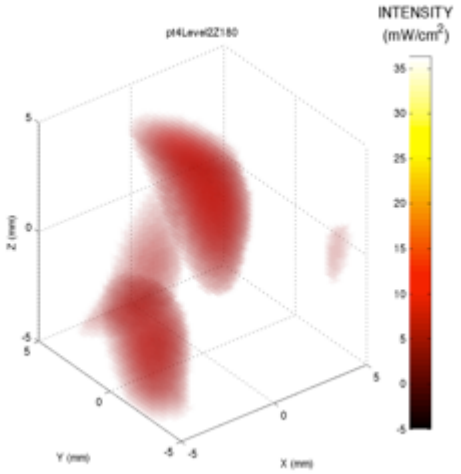

Figure 27: 3D Intensity, Column 4, Level 2, Z180, Cube 1.

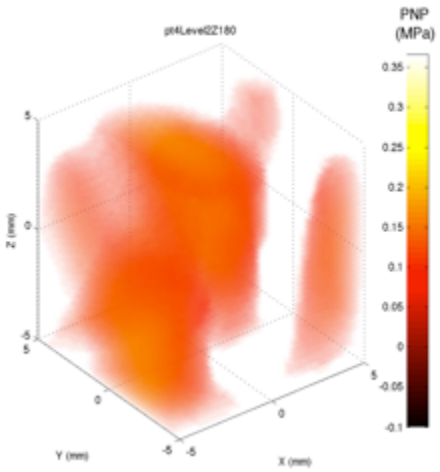

Figure 28: 3D PNP, Column 4, Level 2, Z180, Cube 1.

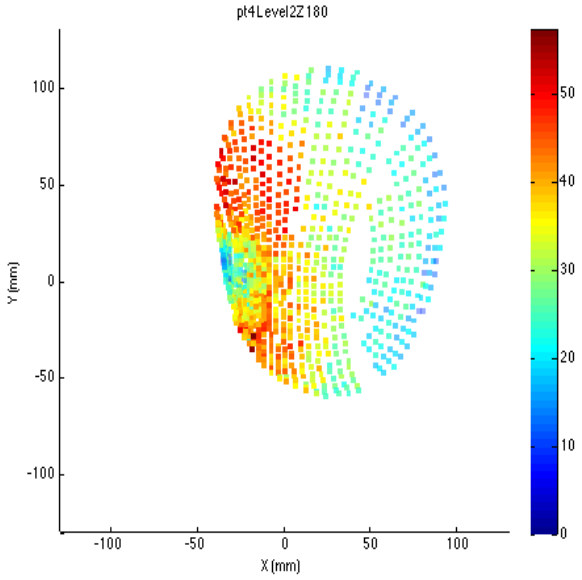

Figure 29: Incident angle, Column 4, Level 2, Z180, Cube 1.

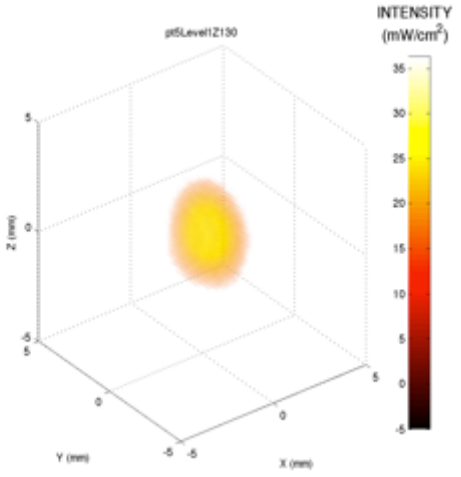

Figure 30: 3D Intensity, Column 5, Level 1, Z130, Cube 2.

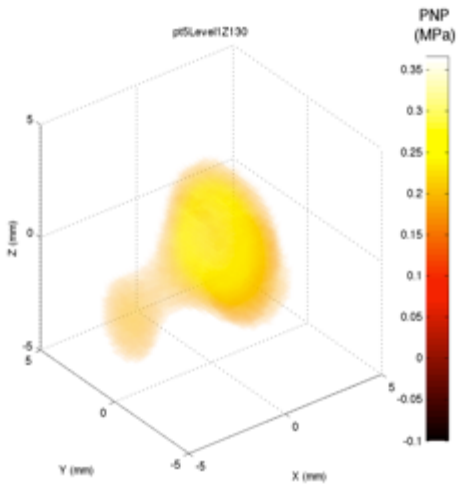

Figure 31: 3D PNP, Column 5, Level 2, Z130, Cube 2.

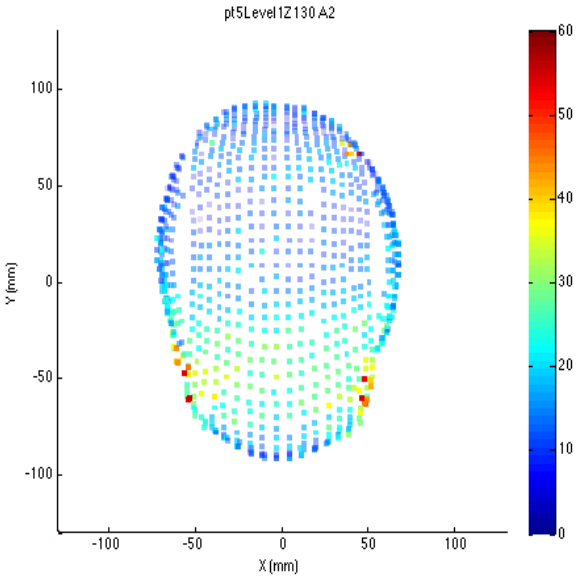

Figure 32: Incident angle, Column 5, Level 1, Z130, Cube 2.

4.1.5 Incident Angles

In addition, for both points the incident angle distributions on the skull surface are shown (Figure 29 and Figure 32). In fact this was calculated for each skull position and target coordinate. The color bar on the right side of the plot shows the incident angle in degrees. Values above 60 degrees are not displayed. After review of these data, what becomes evident is that the intensity strength and geometry is highly affected by even subtle changes of the incident angle distribution. Regarding the incident angle plots, values less than 30 degrees are colored primarily light to dark blue. These angles are those for which longitudinal acoustic transmission is the primary mode, and also the major contributor to the field at the focus. As such, the blue regions of the incident angle

distribution may be considered to be an acoustic “aperture” or “lens” on the skull. Figure 33 and 34 show a sample for the focal zone and the corresponding incident angle distribution.

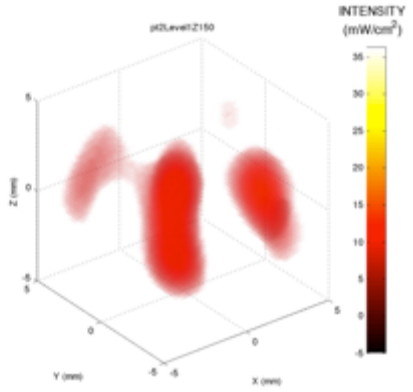

Figure 33: 3D intensity, Column 2, Level 1, Z150, Cube 2.

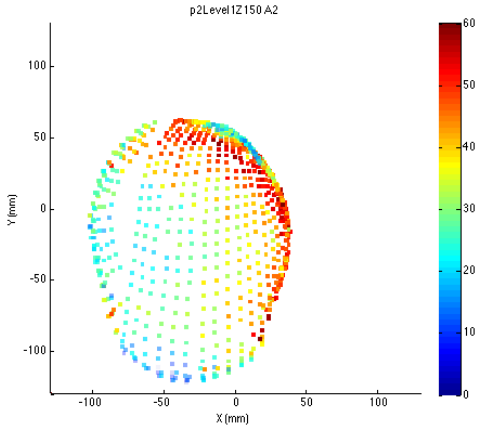

Figure 34: Incident angle, Column 5, Level 1, Z130, Cube 2.

4.1.6 Measurement Columns

To visualize the TEs we plotted all cubes of the five *measurement column*s at once. The colors of the cubes are the results of different maxima in intensity or PNP within each cube. As listed in Table 5 and 6 we calculated the maxima of each cube. In this case we used the overall maxima to scale colors. The results are visualized in Figure 35 – 38.

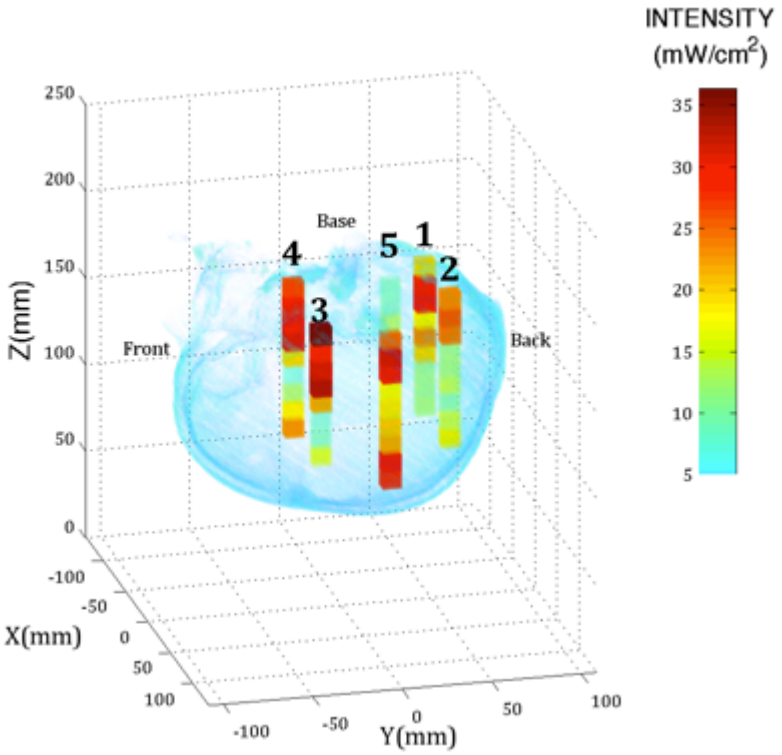

Figure 35: Intensity measurement cubes within *Skull 1* (view: from the front/right). The color bar shows that red Cubes have the highest values.

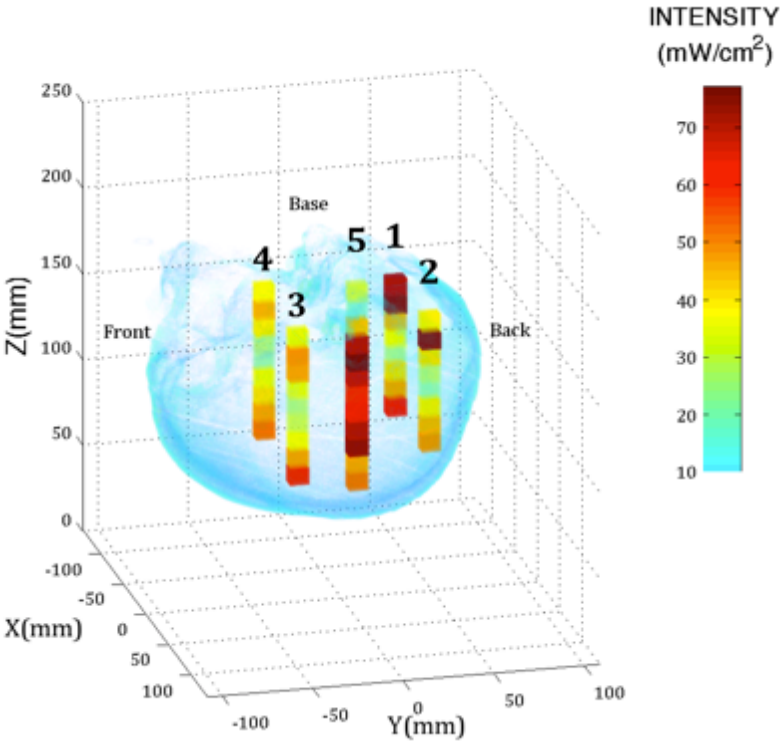

Figure 36: Intensity measurement cubes within *Skull 2* (view: from the front/right). The color bar shows that red cubes have the highest values.

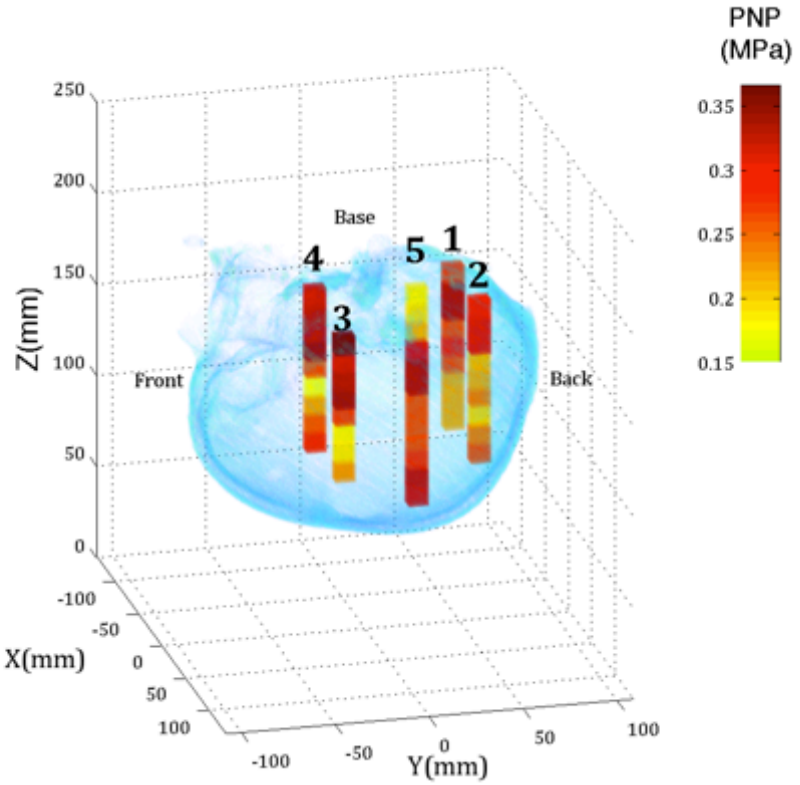

Figure 37: PNP measurement cubes within *Skull 1* (view: from the front/right). The color bar shows that red cubes have the highest values.

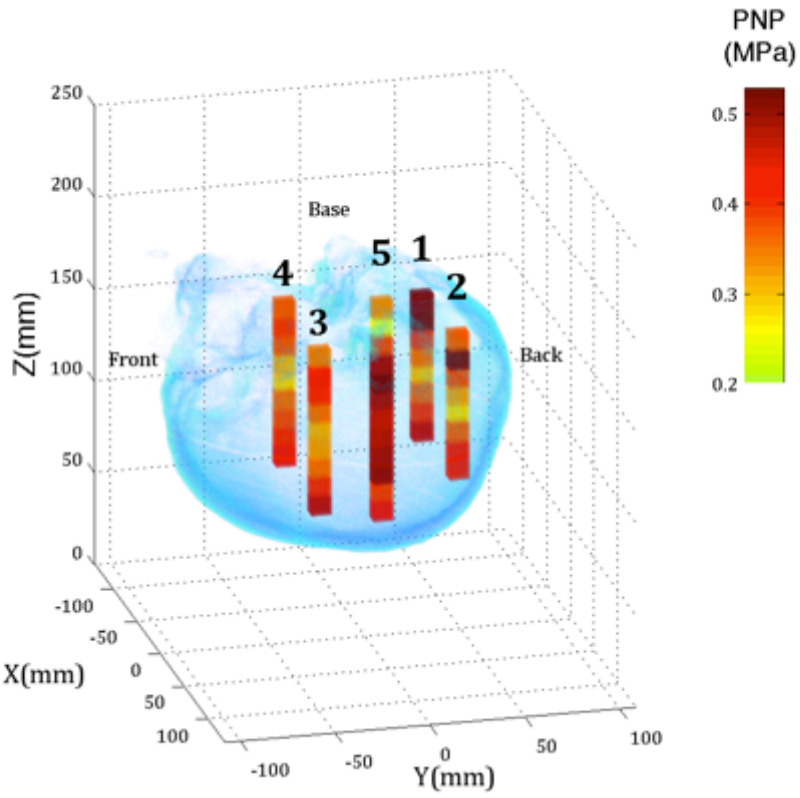

Figure 38: PNP measurement cubes within *Skull 2* (view: from the front/right). The color bar shows that red cubes have the highest values.

As explained in 3.5.1 we used the Delaunay Triangulation to interpolate the collected data. The results are shown in Figure 39 - 42.

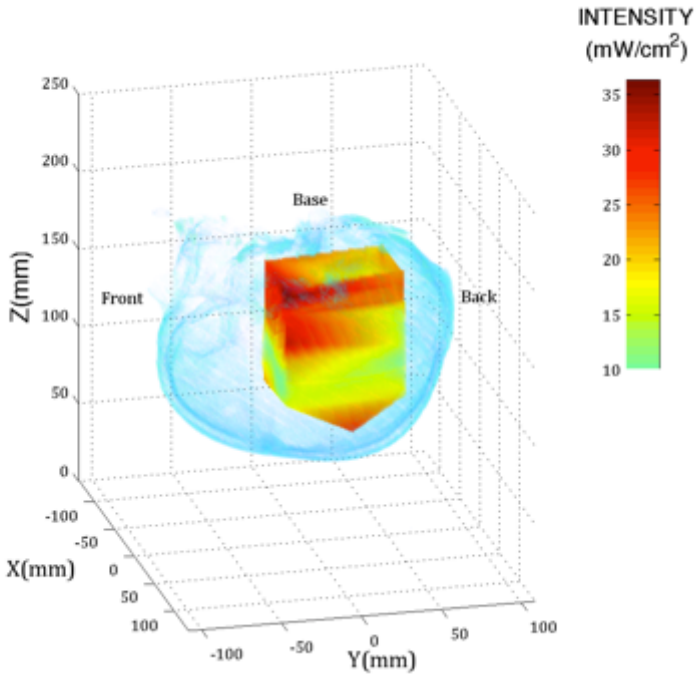

Figure 39: Interpolation of intensity values of measurement cubes within *Skull 1* (view: from the front/right).

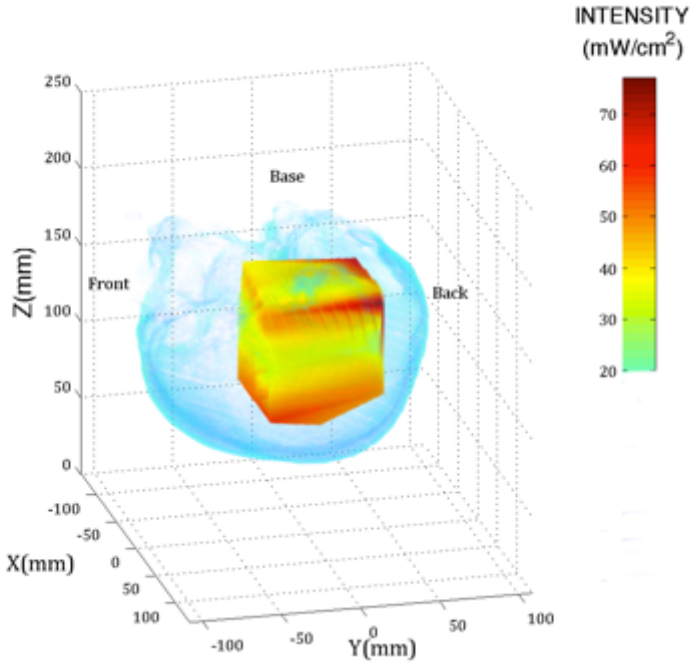

Figure 40: Interpolation of intensity values of measurement cubes within *Skull 2* (view: from the front/right).

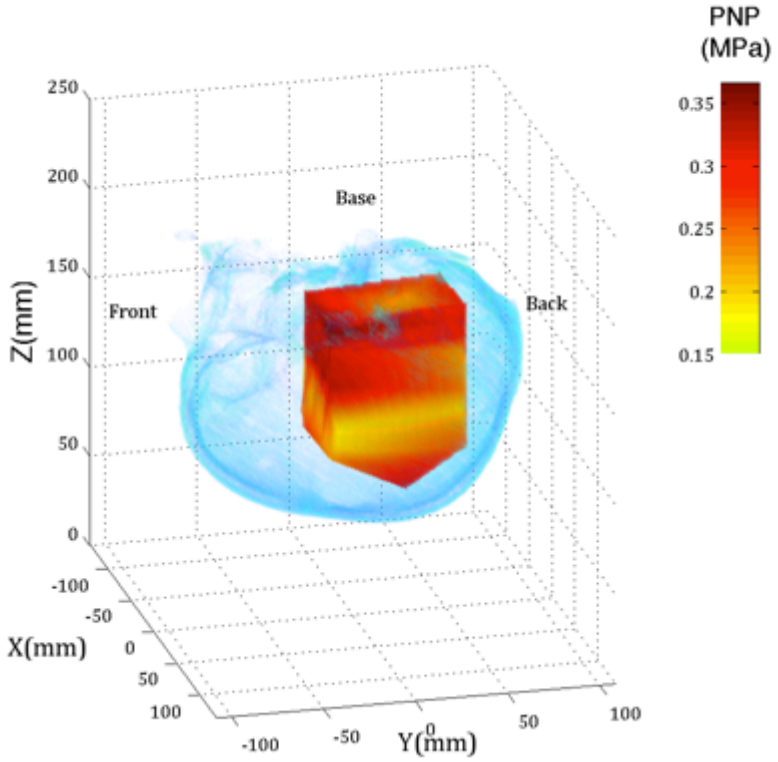

Figure 41: Interpolation of PNP values of measurement cubes within *Skull 1* (view: from the front/right).

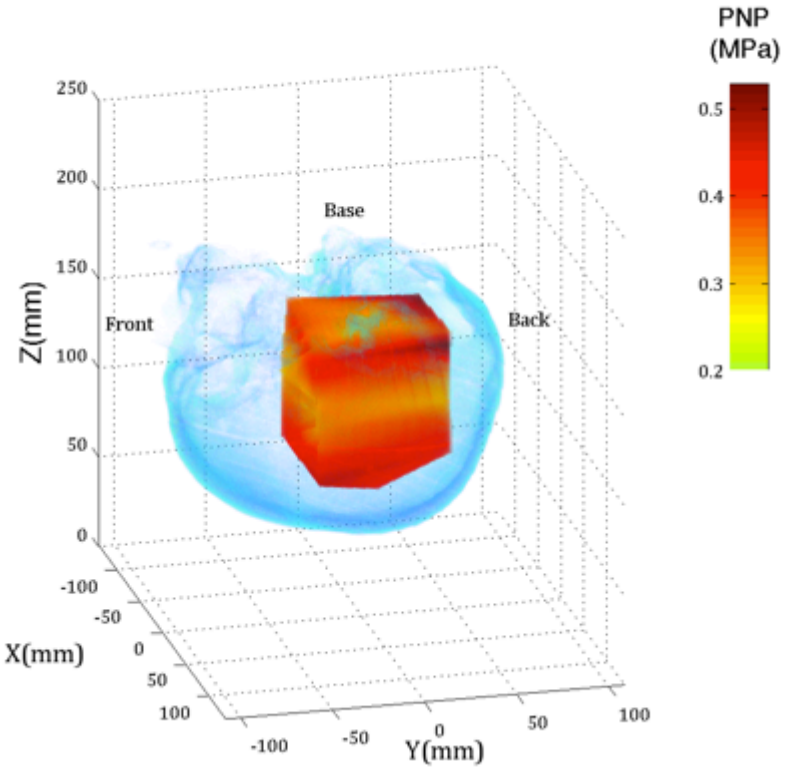

Figure 42: Interpolation of PNP values of measurement cubes within *Skull 2* (view: from the front/right).

4.2 Cavitation Studies

Various 3D-visualisation methods of the PNP distribution along the tube helped to analyze the data. Figure 43 shows a cut through the skull and the interpolated PNP data in top view. The cut is made along the tubing whereas the x-, y-components are parallel to the x-, y-axis. That means the plane is only tilted to the same degree in z-direction as the tube. In Figure 43 the black line represents the tube that starts in the upper right corner and runs through an area of high (center of the volume) and of low (lower left corner) PNP. Figure 44 shows the same slice as Figure 43 but from a different perspective.

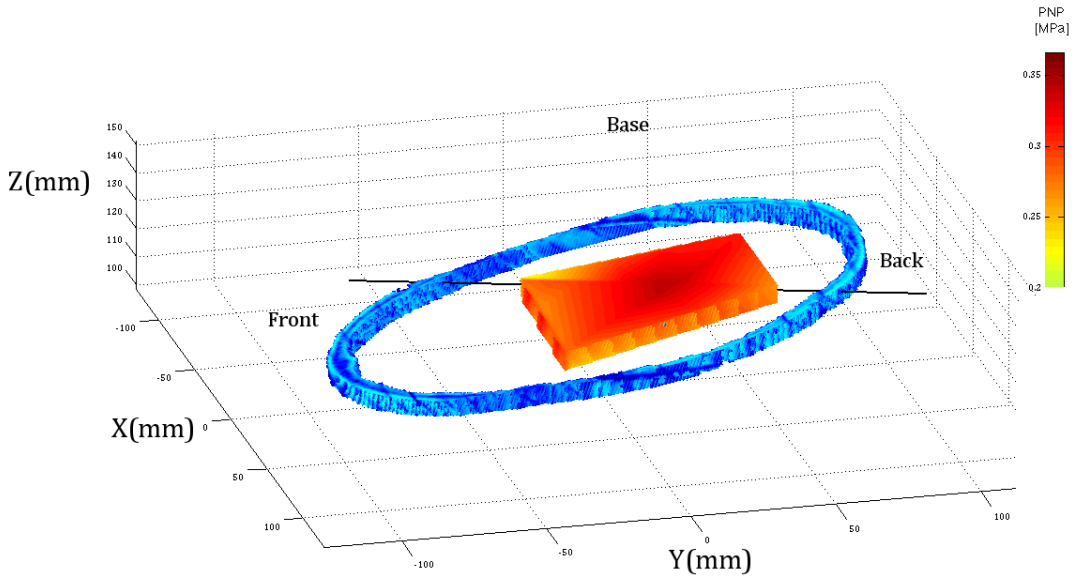

Figure 43: Sliced volume that contains tube (black line) (view: from the front/right).

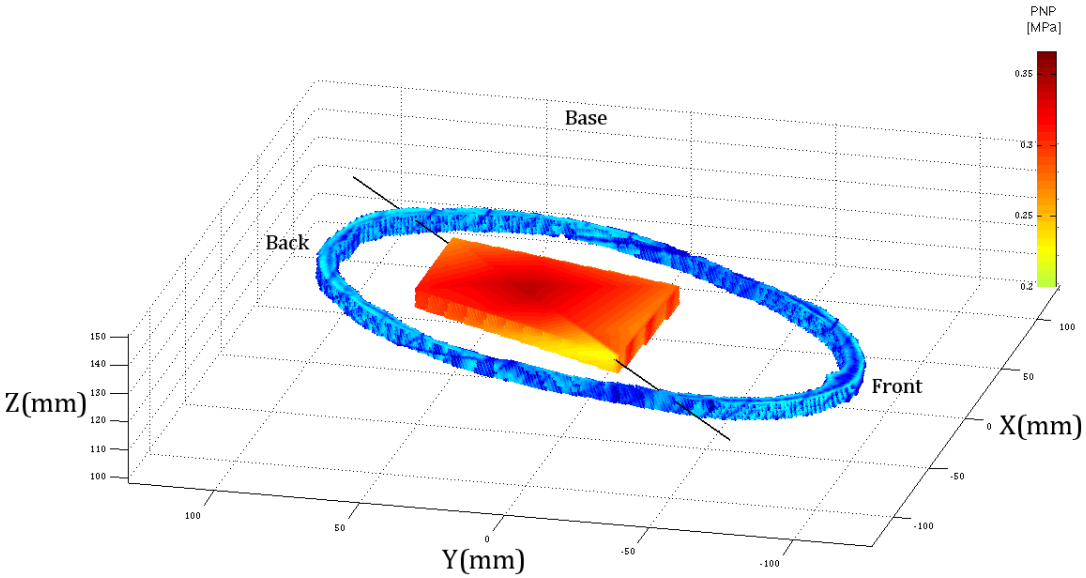

Figure 44: Sliced volume that contains tube (black line) (view: from the front/left).

Furthermore, a MATLAB code created Figure 45 and 46 that show the tube (black line) through the two desired cubes from two different perspectives. *Cube 1* appears in yellow (low PNP), *Cube 2* in red (high PNP). For information on the cube locations see 3.4.4.b.

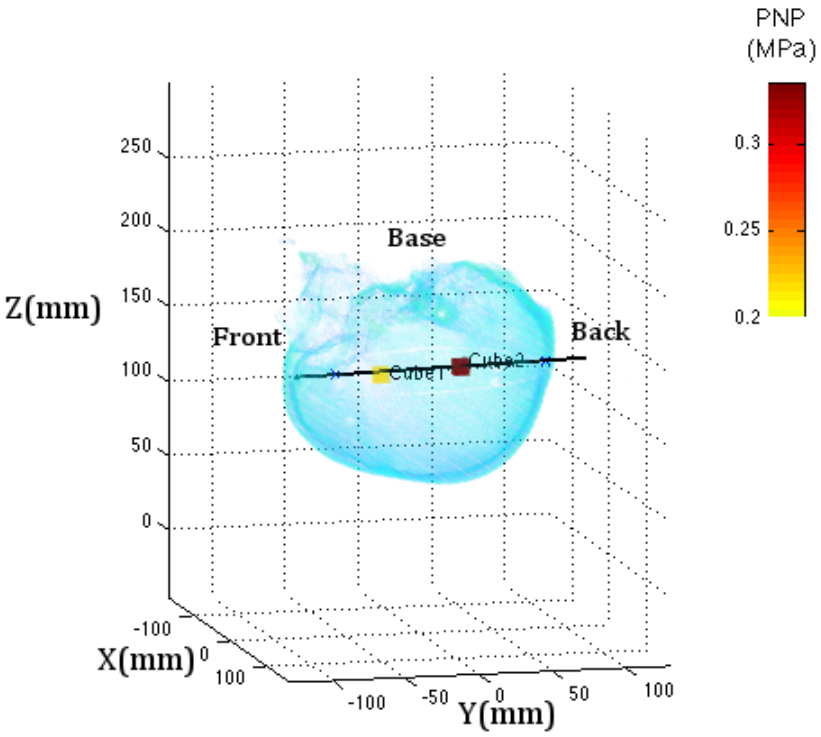

Figure 45: Tube (black line) through Cube 1 and 2 (view: from the front/right).

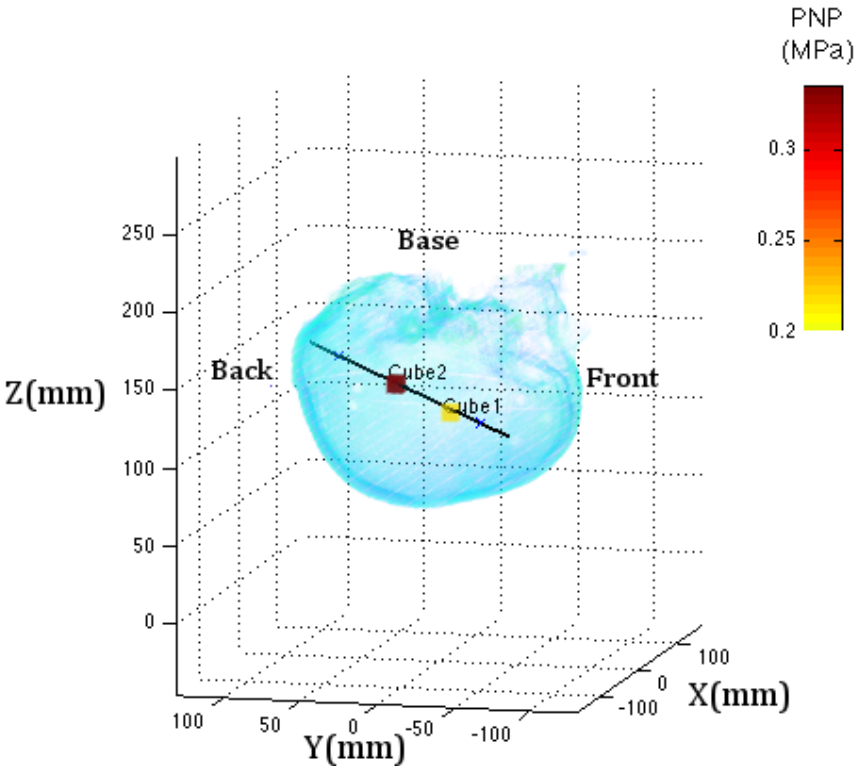

Figure 46: Tube (black line) through Cube 1 and 2 (view: from the front/left).

As explained in 3.5.5, for demonstration the "0" or "1" scores for focus 5, *Column 4*, *Level 2* and Br38 MB at various power values are listed in Table 7. The threshold for *stable cavitation* has been defined as the lowest power level at which a "1" has been assigned to the subharmonic, 1st ultraharmonic, 2nd harmonic, and 3rd harmonic. In the table if a score of "1" is assigned this correlates to a circled point on the spectrum, marking presence of a peak.

Table 7: Example of a *cavitation* identification table. The first column is the acoustic power (AP) of the FUS in units of Watt (W). The next columns show the indicators for the peaks in the frequency spectrum, whereas it starts with the subharmonic (S), followed by the 1st ultraharmonic(U), the 2nd harmonic(2), the 2nd ultraharmonic (u), the 3rd harmonic(3). The threshold at an AP of 103.4 W is highlighted in yellow.

AP[W]	S	U	2	u	3
34.5	0	0	1	0	1
69.0	0	0	1	0	1
75.9	1	0	1	0	1
82.8	1	0	1	0	1
89.7	1	0	1	0	1
103.4	1	1	1	0	1
110.3	1	1	1	0	1
117.2	1	0	1	0	1
124.1	0	1	1	0	1
131.0	0	1	1	0	1
137.9	1	1	1	0	1
144.8	0	1	1	0	1
151.7	0	1	1	0	1
158.6	1	1	1	0	1
165.5	1	1	1	0	1
172.4	0	1	1	0	1
206.9	1	1	1	0	1

Table 8: Thresholds in acoustic power (AP_{Thres}) and PNP in units of Pascal (Pa) for cavitation in Cube 1 under application of MBs (Bracco 38 (BR38)) or water (H_2O).

Media	AP_{Thres} [W]	PNP[kPa]
Br38	103.4	1013,15
H_20	137.9	1169,88

Table 9: Thresholds in acoustic power (AP_{Thres}) and PNP in units of Pascal (Pa) for *cavitation* in Cube 2 under application of MBs (Bracco 38 (BR38)) or water (H_2O).

Media	AP_{Thres} [W]	PNP[kPa]
Br38	48.3	692,11
H_2O	69.0	827,23

Table 8 shows the *acoustic power* (AP) (in W) and PNP (in kPa) threshold for *cavitation* for water (H_2O) either with or without the application of BR 38 MB for *Cube 1*, whereas Table 9 shows the same parameters, but for *Cube 2*. Figure 47-49 compare three spectra with each other as an example for the measurements in *Cube 1* with Br38 as medium. In

the first spectrum there is no indication for a *cavitation* event, in the second figure the power is set to threshold, for the third one above threshold.

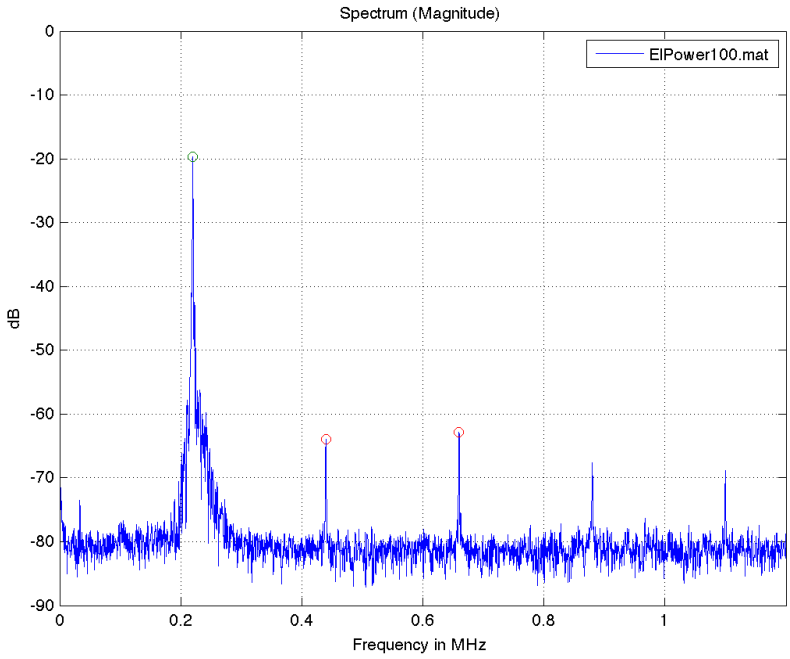

Figure 47: Spectrum for AP of 69.0 W (equals electric power of 100 W) and Br38 as medium. There are no indications for *cavitation*.

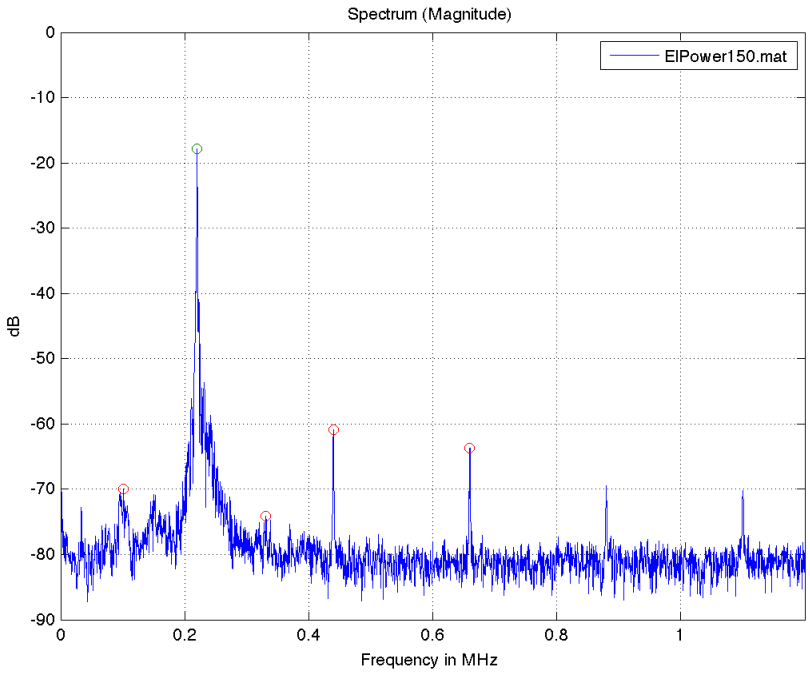

Figure 48: Spectrum for AP of 103.4 W (equals electric power of 150 W) and Br38 as medium. The subharmonic, 1st ultraharmonic, 2nd harmonic, and 3rd harmonic indicate presence of *cavitation*. 103.4 W AP was defined as the threshold for *cavitation*.

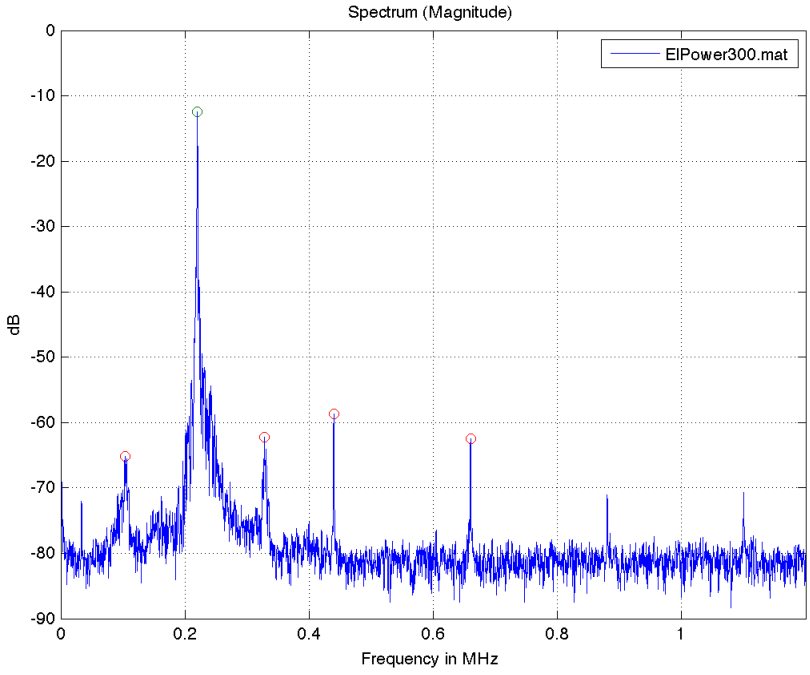

Figure 49: Spectrum for AP of 206.9 W (equals electric power of 300 W) and Br38 as medium. The AP is twice the threshold. The subharmonic and 1st ultraharmonic are very prominent.

The PNP distribution along the tube is shown in Figure 50. In MATLAB the tube can be rotated in x-, y- and z-direction. The red color in the center of the tube (*Cube 2*) indicates high PNP, the yellow area (especially in at *Cube 1*) indicates low PNP.

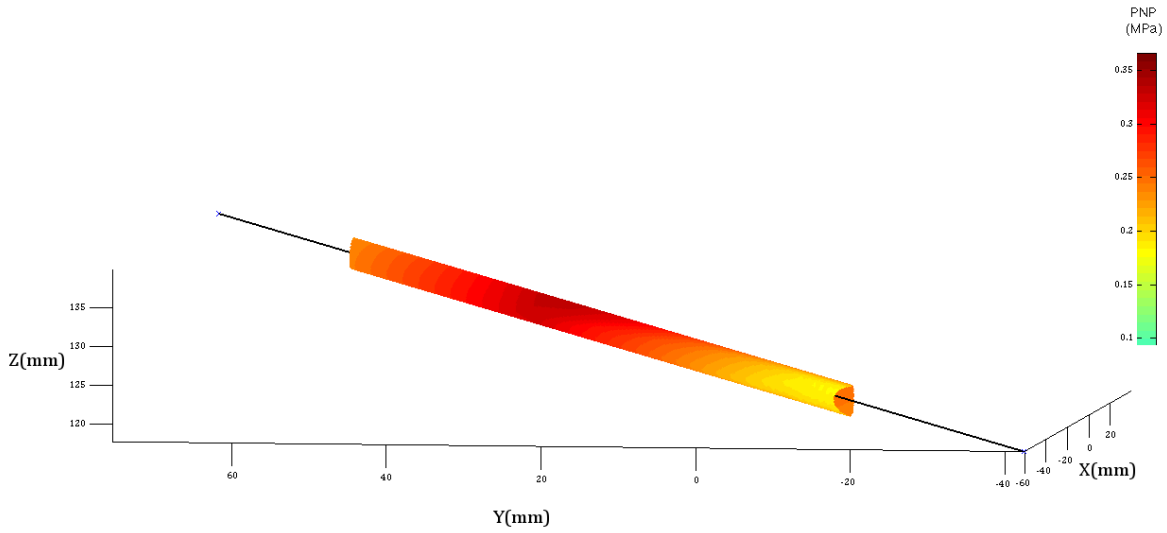

Figure 50: PNP distribution along the tube (view: from the front/left).

5 Discussion and Conclusion

Although the definition of the TEs demands fundamental research the outcome provides an exceptional content of information for any studies on *cavitation*.

5.1 Treatment Envelope Studies

Studies on the acoustic intensity and PNP distribution within the skulls were necessary to define the TEs. This characterization of the ultrasound field configuration is of inestimable value for the following *cavitation* studies.

Results of the TE measurements keep options to interpret the shape of the focal zone open. Nevertheless the 3D plots show that when there is a significant distortion of the focal volume, there is often an asymmetric distribution of the acoustic aperture on the skull (compare Figure 27 – 29 to 30-32).

It is also instructive to examine the data for *measurement column 5* for both skulls. *Column 5* is composed of scans made through the foramen magnum access hole, centrally located in the skull base. For this *measurement column*, there is much less distortion of the focal volumes as compared to scans in the other columns. That is not to say that no points on *Column 5* fall below the *"thermal-therapy"* TE boundary, as a glance at Table 5 and 6 show. For both skulls there is a region toward the base along *Column 5* that has lower intensity values.

When comparing the 3D scans from *Skulls 1 & 2*, there are considerable differences in the focal shapes, intensity and PNP values at equivalent measurement volumes. However, for both skulls the angle distributions are remarkably similar, as a side-by-side comparison along the *measurement column*s demonstrates. This indicates that the skulls had very similar overall geometry, and additional measurements revealed similar density and thickness values. This suggests that subtle differences in the manner that the acoustic energy passes through the skull may have significant effects on the resulting focal zone. These differences would be accentuated for intensity measurements, which are proportional to the square of the pressure field.

Another interesting point to note is that for the majority of the measurements for which the peak falls below half-maximum, we see that there is considerable distortion of the acoustic field. For *Skull 1*, 13 of the 16 measurements, for *Skull 2*, 10 of 15 measurements in this category exhibit this behavior. For most of these this occurs in *measurement columns 1-4*, meaning lateral translation of the skulls was involved. It

seems likely then that this lateral translation sets up asymmetries in acoustic apertures on the skull, and this in turn leads to focal distortion and loss of acoustic intensity.

This observation suggests that the TEs may be enhanced or extended if 1) the incident angle distribution was more symmetric on the skull, or 2) if the transmission of ultrasound was limited to a single aperture. In the first case, this may be accomplished if instead of mechanically translating the skull in order to position the acoustic focal volume, the skull would have been rotated and/or tilted. This should have the effect of keeping the incident angle distribution (and hence the acoustic aperture) more centrally located on the calvarium and minimize the focal distortions. In the second case, one that envisions lateral skull translation, it may be possible to simply turn off selected transducer elements and thereby eliminate one or more of the competing (and interference – causing) acoustic apertures. Both of these strategies could be evaluated in a subsequent study.

5.2 Cavitation Studies

All major decisions related to *cavitation* measurements, like the positioning of the tube, the applied power by the FUS and the positioning of the skull were based on previous research done for the TE within this thesis.

Different approaches to detect *cavitation* passively are documented in literature. The method in this thesis used to search for peaks in the *cavitation* studies (3.5.5) is similar to the one documented by Farny, Holt et al. (2008). Instead of multiplying the standard deviation of the frequency spectrum by 3 and calculate the difference between the result and the main background signal, we decided to calculate the difference between the main background signal and the peaks amplitude. Calculations for various spectra have shown, that the approach by Farny, Holt et al. (2008) is very similar to our approach. We therefore decided to detect *cavitation* in the way showed in 3.5.5.

It is shown in this thesis that the presence of the subharmonic and first ultraharmonic is a robust indicator of *stable cavitation*. Furthermore, it is demonstrated (Table 7) that the regular harmonics are present with or without *cavitation*, on the contrary the 2nd ultraharmonic is hardly significant in presence. That illustrates that the presence of harmonics is not an indicator of *stable cavitation*, but rather non-linear acoustic propagation through the medium. A reason for the fact that "1" is rarely assigned to the 2nd ultraharmonic is probably the frequency range of the PCD sensor and the voltage scale setting on the scope which kind of determines the noise baseline. As a

matter of fact the instruments are not optimized to acquire very small signals but if the fundamental could be filtered out the presence of the 2nd ultraharmonic would increase. As a conclusion due to the presence of the regular harmonics with or without *cavitation*, these signals are superfluous and can be disregarded.

It might questionable why in the case of *Skull 1* (Table 5) the highest intensity value is located at the same position as the maximum PNP (i.e. *Level 1/Column 3/Z170*), whereas in contrary to that for *Skull 2* these two maxima appear at different spots within the skull ($intensity_{max}$: *Level 1/Column 5/Z140*, PNP_{max}: *Level 1/Column 2/Z160*). In AIMS intensity and PNP are calculated differently based on the acquired signal by the hydrophone. Intensity is in fact calculated from the *root-mean-square pressure* (Prms). PNP and Prms are different types of pressure and may not be equally localized due to the density of water that affects the speed of sound and hence the phasing.

5.3 Comparision between "Thermal-Therapy" and "Mechanical-Therapy" Treatment Envelope

Data acquired within these studies allows defining both, the *"thermal-therapy"* and the *"mechanical-therapy"* TE, but in this thesis only the first one was determined. Nevertheless, results shown in Table 5 and 6 indicate that the *"mechanical-therapy"* TE is larger than the *"thermal-therapy"* TE. Defining the *"mechanical-therapy"* TE boundaries in the same way as for the *"thermal-therapy"* TE (3.5.1) leads to the result that only one PNP value per skull (compare to intensity *Skull 1*: 16 and *Skull 2*: 15) is located outside the envelope. Mathematically this is reasonable since the intensity is proportional to the square of the PNP.

6 Summary

All the measurements were done on a set of two human cadaver skulls. The performed research addressed the effects caused by therapeutic ultrasound: the thermal and the non-thermal (mechanical) effect. Therefore the underlying physical properties intensity (thermal effect) and *peak negative pressure* (non-thermal effect) were observed. Based on the results the boundaries of two volumes, treatment envelopes (TE), per skull were defined. These volumes were termed *"thermal-therapy"* TE and *"mechanical-therapy"* TE depending on the causing mechanism. By fundamental research within this thesis the difference between the envelopes was pointed out. The expected main difference, i.e. the larger size of the *"mechanical-therapy"* compared to the *"thermal-therapy"* TE, was examined and proved with special focus on the mechanical effect of *cavitation*. As a matter of fact the *"mechanical-therapy"* TE was the reason to design measurements for *passive cavitation detection* (PCD). PCD measurements were performed with and without *microbubbles* (MB), thus showing the influence of MB on the *cavitation* threshold. It was demonstrated that the application of MBs reduces the threshold in *peak negative pressure* needed to cause a *cavitation* event. PCD was not only necessary to confirm the shape of the TE, conducted measurements might also be of considerable value to any transcranial FUS application as they show that mechanical based therapy (e.g. *cavitation*, particularly with MBs) may be applied to brain regions beyond the capability of thermal based applications (e.g. tumor ablation).

Although it is still a long way until therapeutic ultrasound is fully adopted in clinical practice this thesis shows that FUS is an innovative technology for non-invasive neurointerventions with enormous potential to help millions of patients, thus emphasizing research in this field.

References

Abramowicz, J. S., S. B. Barnett, A. F. Duck, P. Edmonds, K. Hynynen and M. Ziskin (2008). "Fetal Thermal Effects of Diagnostic Ultrasound." Journal of Ultrasound in Medicine **27**(4): 541-559.

Ashokkumar, M., M. Hodnett, B. Zeqiri, F. Grieser and G. J. Price (2007). "Acoustic Emission Spectra from 515 kHz Cavitation in Aqueous Solutions Containing Surface- Active Solutes." J Am Chem Soc **129**: 2250-2258.

Aubry, J.-F., L. Marsac, M. Pernot, B. Robert, A.-L. Boch, D. Chauvet, N. Salameh, L. Souris, L. Darasse, J. Bittoun, Y. Martin, C. Cohen-Bacrie, J. Souquet, M. Fink and M. Tanter (2010). "High intensity focused ultrasound for transcranial therapy of brain lesions and disorders " IRBM **31**(2): 87-91.

Aubry, J.-F., M. Tanter, M. Pernot, J. L. Thomas and M. Fink (2003). "Experimental demonstration of noninvasive transskull adaptive focusing based on prior computed tomography scans." J Acoust Soc Am **113**(1): 84.

Bader, K. B. and C. K. Holland (2012). "Gauging the likelihood of stable cavitation from ultrasound contrast agents." Phys Med Biol **58**(1): 127-144.

Bailey, M. R., V. Khokhlova, O. A. Sapozhnikov, S. G. Kargl and L. A. Crum (2003). "Physical Mechanisms of the Therapeutic Effect of Ultrasound." Acoustical Physics **49**(4): 369-388.

Barnett, S. B., H.-D. Rott, G. R. Ter Haar, M. Ziskin and K. Maeda (1997). "The Sensitivity of Biological Tissue To Ultrasound." Ultrasound Med Biol **23**(6): 805-812.

Baron, C., J.-F. Aubry, M. Tanter, S. Meairs and M. Fink (2009). "Simulation of intracranial acoustic fields in clinical trials of sonothrombolysis." Ultrasound Med Biol **35**(7): 1148-1158.

Behrens, S., K. Spengos, M. Daffertshofer, H. Schroeck, C. E. Dempfle and M. Hennerici (2001). "Transcranial ultrasound-improved thrombolysis: diagnostic vs. therapeutic ultrasound." Ultrasound Med Biol **27**(12): 1683-1689.

Billard, B. E., K. Hynynen and R. B. Roemer (1989). "Effects of physical parameters on high temperature ultrasound hyperthermia." Ultrasound Med Biol **16**(4): 409-420.

Broderick, J. P., Y. Y. Palesch, A. M. Demchuk, S. D. Yeatts, P. Khatri, M. D. Hill, E. C. Jauch, T. G. Jovin, B. Yan, F. L. Silver, R. von Kummer, C. A. Molina, B. M. Demaerschalk, R. Budzik, W. M. Clark, O. O. Zaidat, T. W. Malisch, M. Goyal, W. J. Schonewille, M. Mazighi, S. T. Engelter, C. Anderson, J. Spilker, J. Carrozzella, K. J. Ryckborst, L. S. Janis, R. H. Martin, L. D. Foster and T. A. Tomsick (2013). "Endovascular Therapy after Intravenous t-PA versus t-PA Alone for Stroke." New England Journal of Medicine **368**(10): 893-903.

Burgess, A., Y. Huang, A. C. Waspe, M. Ganguly, D. E. Goertz and K. Hynynen (2012). "High-intensity focused ultrasound (HIFU) for dissolution of clots in a rabbit model of embolic stroke." PLoS One **7**(8): e42311.

Bushberg, J. T., J. A. Seibert, E. M. Leidholdt and J. M. Boone (2001). Diagnostic Radiology. The Essential Physics of Medical Imaging**:** 356.

Ciccone, A., L. Valvassori, M. Nichelatti, A. Sgoifo, M. Ponzio, R. Sterzi and E. Boccardi (2013). "Endovascular Treatment for Acute Ischemic Stroke." New England Journal of Medicine **368**(10): 904-913.

Coakley, W. T. and W. L. Nyborg (1978). Cavitation; dynamics of gas bubbles; applications. Ultrasound: Its Applications in Medicine and Biology. F. J. Fry, Elsevier, New York**:** 77-159.

Deane, C. and C. Lees (2000). "Doppler obstetric ultrasound: a graphical display of temporal changes in safety indices." Ultrasound in Obstetrics and Gynecology **15**: 418-423.

Dijkmans, P. A., L. J. Juffermans, R. J. Musters, A. van Wamel, F. J. ten Cate, W. van Gilst, C. A. Visser, N. de Jong and O. Kamp (2004). "Microbubbles and ultrasound: from diagnosis to therapy." Eur J Echocardiogr **5**(4): 245-256.

Ensminger, D. and L. J. Bond (2011). Elastic Wave Propagation and Associated Phenomena. Ultrasonics: Fundamentals, Technologies, and Applications, Third Edition, CRC Press.

Ensminger, D. and L. J. Bond (2011). Safety and Therapeutic Applications. Ultrasonics: Fundamentals, Technologies, and Applications, Third Edition, CRC Press.

Farny, C. H., R. G. Holt and R. A. Roy (2008). "Temporal and spatial detection of HIFU-induced inertial and hot-vapor cavitation with a diagnostic ultrasound system." Ultrasound Med Biol **35**(4): 603-615.

Franc, J.-P. (2007). The Rayleigh-Plesset equation: a simple and powerful tool to understand various aspects of cavitation. Fluid Dynamics of Cavitation and Cavitating Turbopumps. L. d'Agostino, Salvetti, M.V. **496:** 1-41.

Francis, A. D., A. C. Baker and H. C. Starritt (1998). Ultrasound in Medicine.

Francis, K., J. van Beek, C. Canova and J. W. Neal (2003). "The Blood Brain Barrier". Retrieved April, 03, 2013, from http://journals.cambridge.org/fulltext_content/ERM/ERM5_15/S1462399403006252sup002.htm.

Frenkel, V. (2010). Therapeutic Ultrasound: Mechanisms to applications, Nova Science Publishers, Inc.

Gallo, J. A., D. O. Draper, L. T. Brody and G. W. Fellingham (2004). "A comparison of human muscle temperature increases during 3-MHz continuous and pulsed ultrasound with equivalent temporal average intensities." J Orthop Sports Phys Ther **34**(7): 395-401.

Hawkins, B. T. and T. P. Davis (2005). "The blood-brain barrier/neurovascular unit in health and disease." Pharmacol Rev **57**(2): 173-185.

Hendee, W. R. (2012). Physics of Thermal Therapy, Fundamentals and Clinical Applications.

Hendee, W. R. and E. R. Ritenour (2002). Ultrasound Waves. Medical Imaging Physics.

Hill, C. R., J. C. Bamber and G. Ter Haar (2005). Ultrasonic Biophysics. Physical Principles of Medical Ultrasonics.

Hoskins, P., K. Martin and A. Thrush (2010). Diagnostic Ultrasound Physics and Equipment**:** 227.

Howard, S. M. and C. I. Zanelli (2007). Characterization of a HIFU Field at High Intensity. Ultrasonics Symposium.

Howard, W. J. and M. Graham (2003). High Speed Signal Propagation**:** 45.

Hsieh, D. and M. S. Plesset (1961). "Theory of Rectified Diffusion of Mass into Gas Bubbles." J Acoust Soc Am **33**(2): 206-215.

Husseini, G. A., M. A. Diaz de la Rosa, E. S. Richardson, D. A. Christensen and W. G. Pitt (2005). "The role of cavitation in acoustically activated drug delivery." J Control Release **107**(2): 253-261.

Hynynen, K. and F. A. Jolesz (1998). "Demonstration of potential noninvasive ultrasound brain therapy through an intact skull." Ultrasound Med Biol **24**(2): 275-283.

Hynynen, K., N. McDannold, N. Sheikov, F. Jolesz and N. Vykhodtseva (2005). "Local and reversible blood-brain barrier disruption by noninvasive focused ultrasound at frequencies suitable for trans-skull sonications." Neuroimage **24**(1): 12-20.

Johns, L. D. (2002). "Nonthermal Effects of Therapeutic Ultrasound: The Frequency Resonance Hypothesis " Journal of Athletic Training **37**(3): 293-299.

Keilman, G. W. and P. J. Kaczkowski (1998). "High Intensity Focused Ultrasound Transducer Design for Surgical and Hemostatic Applications." J Acoust Soc Am **103**(5): 2831-2831.

Lecoffre, Y. (1997). Pheonomenon of Cavitation. Cavitation: Bubble Trackers.

McDannold, N., C. D. Arvanitis, N. Vykhodtseva and M. S. Livingstone (2012). "Temporary disruption of the blood-brain barrier by use of ultrasound and microbubbles: safety and efficacy evaluation in rhesus macaques." Cancer Research **72**(14): 3652-3663.

McDannold, N., G. T. Clement, P. Black, F. Jolesz and K. Hynynen (2010). "Transcranial magnetic resonance imaging- guided focused ultrasound surgery of brain tumors: initial findings in 3 patients." Neurosurgery **66**(2): 323-332.

Merz, E. (2002). Ultrasound in Obstetrics and Gynecology.

Nyborg, W. L. (1965). "Acoustic streaming." Physical Acoustics **2**: 265-331.

Nyborg, W. L. (1981). "Heat generation by ultrasound in a relaxing medium." J Acoust Soc Am **70(2)**: 310-312.

Petit, B., E. Gaud, D. Colevret, M. Arditi, F. Yan, F. Tranquart and E. Allemann (2012). "In vitro sonothrombolysis of human blood clots with BR38 microbubbles." Ultrasound Med Biol **38**(7): 1222-1233.

Pichardo, S., V. W. Sin and K. Hynynen (2011). "Multi-frequency characterization of the speed of sound and attenuation coefficient for longitudinal transmission of freshly excised human skulls." Phys Med Biol **56**(1): 219-250.

Quistgaard, J. U., C. Desilets and P. Martin (2010). "High Intensity Focused Ultrasound." The European Aesthetic Guide.

Rosenschein, U., V. Furman, E. Kerner, I. Fabian, J. Bernheim and Y. Eshel (2000). "Ultrasound Imaging-Guided Noninvasive Ultrasound Thrombolysis : Preclinical Results." Circulation **102**(2): 238-245.

Salgaonkar, V. A., S. Datta, C. K. Holland and T. D. Mast (2009). "Passive cavitation imaging with ultrasound arrays." J Acoust Soc Am **126**(6): 3071-3083.

Tanter, M., J. L. Thomas and M. Fink (1998). "Focusing and steering through absorbing and aberrating layers: application to ultrasonic propagation through the skull." J Acoust Soc Am **103**(5 Pt 1): 2403-2410.

Ter Haar, G. R. (2001). "Acoustic Surgery." Physics today **54**(12): 29-34.

Tobias, J., K. Hynynen, R. Roemer, A. N. Guthkelch, A. S. Fleischer and J. Shively (1987). "An ultrasound window to perform scanned, focused ultrasound hyperthermia treatments of brain tumors." Med Phys **14**(2): 228-234.

Tu, J., J. Ha Hwang, T. Chen, T. Fan, X. Guo, L. A. Crum and D. Zhang (2012). "Controllable in vivo hyperthermia effect induced by pulsed high intensity focused ultrasound with low duty cycles." Applied Physic Letters **101**(12): 124102.

Tunc, M. and C. F. Delale (2003). Energy Dissipation due to Fission of Cavitating Bubbles. Fifth International Symposium on Cavitation. Osaka, Japan.

Veltkamp, R. (2012). "Akuttherapie des ischämischen Schlaganfalls". Retrieved April, 03, 2013, from http://www.dgn.org/leitlinien-online-2012/inhalte-nach-kapitel/2310-ll-22-2012-akuttherapie-des-ischaemischen-schlaganfalls.html.

Vykhodtseva, N. (2010). "Disruption of Blood–Brain Barrier by Focused Ultrasound for Targeted Drug Delivery to the Brain." Neuromethods **45**: 35-62.

White, P. J., G. T. Clement and K. Hynynen (2006). "Longitudinal and shear mode ultrasound propagation in human skull bone." Ultrasound Med Biol **32**(7): 1085-1096.

Wu, J. and W. L. Nyborg (2008). "Ultrasound, cavitation bubbles and their interaction with cells." Advanced Drug Delivery Reviews **60**(10): 1103-1116.

Yin, X. and K. Hynynen (2005). "A numerical study of transcranial focused ultrasound beam propagation at low frequency." Phys Med Biol **50**(8): 1821-1836.

Zeiler, K. and E. Auff (2007). Klinische Neurobiologie 2.

Figures

Figures

Tables

Abbreviations

AC	ALTERNATING CURRENT
ACD	ACTIVE CAVITATION DETECTION
ACT	ACOUSTIC CORRECTION TABLE
AIMS	ACOUSTIC INTENSITY MEASUREMENT SYSTEM
AP	ACOUSTIC POWER
BBB	BLOOD-BRAIN BARRIER
BURL	BRAIN ULTRASOUND RESEARCH LABORATORY
CNS	CENTRAL NERVOUS SYSTEM
COL	COLUMN
CT	COMPUTED TOMOGRAPHY
CW	CONTINOUS WAVE
DICOM	DIGITAL IMAGING AND COMMUNICATIONS IN MEDICINE
DIV	DIVISION
DW-MRI	DIFFUSION-WEIGHTED-MAGNETIC RESONANCE IMAGING
EMB	ENCAPSULATED MICROBUBBLE
FFT	FAST FOURIER TRANSFORM
FUS	FOCUSED ULTRASOUND
HU	HOUNSFIELD UNIT
ITA	TEMPORAL AVERAGE INTENSITY
L	LEVEL
MB	MICROBUBBLE
MI	MECHANICAL INDEX
MRI	MAGNETIC RESONANCE IMAGING
NIHSS	NATIONAL INSTITUTE OF HEALTH STROKE SCALE
PCD	PASSIVE CAVITATION DETECTION
PNP	PEAK NEGATIVE PRESSURE
PPP	PEAK POSITIVE PRESSURE
PRMS	PRESSURE ROOT-MEAN-SQUARE
PW	PULSED-WAVE
R-TPA	RECOMBINANT-TISSUE PLASMINOGEN ACTIVATOR
TCMRGFUS	TRANSCRANIAL MAGNETIC RESONANCE IMAGING-GUIDED FOCUSED ULTRASOUND
TE	TREATMENT ENVELOPE
TPA	TISSUE PLASMINOGEN ACTIVATOR